ABSTRACT

Title of Document: HARMONIC VIBRATION TESTING OF ELECTRONIC COMPONENTS ATTACHED TO PRINTED WIRING BOARDS WITH SAC305 AND EUTECTIC SnPb SOLDER

Beth Miller Paquette, Master of Science, 2010

Directed By: Professor Donald B. Barker,
Department of Mechanical Engineering

Ball grid arrays attached to printed wiring boards with conventional tin-lead solder (63/37) and one of the leading lead-free tin-silver-copper solders (SAC305) were tested at high and low load levels of harmonic vibration. Leadless chip resistors attached to printed wiring boards with conventional tin-lead solder and lead-free solders (SAC105 and SAC305, and tin-nickel-copper, SN100C) were tested at low levels of harmonic vibration. The tests were conducted near the natural frequency of the assemblies to accelerate testing and to generate high cycle fatigue failures in a reasonable amount of time. The results showed that there are nearly negligible differences in the high cycle fatigue life between the SnPb and SAC305 solders. SN100C and SAC105 were less durable. A master durability plot was generated for

SAC305 and SnPb to confirm the negligible-difference between the solders. A safe area was defined be used as a design goal for survivablity for circuit board design.

HARMONIC VIBRATION TESTING OF ELECTRONIC COMPONENTS ATTACHED TO PRINTED WIRING BOARDS WITH SAC305 AND EUTECTIC SnPb SOLDER

By

Beth Miller Paquette

Thesis submitted to the Faculty of the Graduate School of the
University of Maryland, College Park, in partial fulfillment
of the requirements for the degree of
Master of Science
2010

Advisory Committee:
Professor Donald Barker, Chair
Dr. Michael Osterman
Professor Peter Sandborn

Dedication

To my father-in-law, Ted Paquette. You were my inspiration for returning to school. You encouraged me to do my best. You were one of the smartest engineers I knew. I, too, hope to have my name on Mars someday.

To my uncle, Bob Miller. You were a true 'October Sky' story. You showed me anything really is possible. Whenever I drive over the Chesapeake Bay, I think of you. After all, it is "The Bridge that Bob Miller Built."

I love and miss you both. May you rest in peace.

Acknowledgements

- To my husband Aaron Paquette: Thank you for your help with my statistical analysis. Thank you for all of the encouragement and helping me back up on my feet after all the rough patches, and putting up with my crazy work schedules. I love you!
- To my parents, Leon and Jo Anne Miller: Thank you for all of your encouragement, and making sure I stay healthy and rested through the stressful parts of grad school.
- To my advisor Dr. Barker: Thank you for the opportunity to work with you for the past 1 1/2 years. It has been a rewarding experience and I definitely learned a lot.
- Thank you to my committee, Dr. Osterman and Professor Sandborn for reviewing my work and being a part of this process.
- Thank you to Nick Willard and Joey Landwehr who helped with the shaker test setup. Thanks Nick for helping with running tests and teaching me how to cross-section.
- To Lee Smith at GCAS: Thank you for providing the BGA boards, and participating in the BGA harmonic testing and analysis.
- Thank you Vikram Srinivas for taking all that time to train me on the shaker.
- Thank you to Anshul and to Bhanu for helping me out with using lab equipment.
- Thank you to "Team Barker": Patrice and Gil, thank you for helping me with cross-sectioning. Rachel, thank you for helping me with board soldering and

running my tests while you were here. I am glad to have met you and I am glad we are friends.

- To my brother Jason Miller: Thank you for helping me with proofreading this thesis and for your encouragement.
- Thank you to the Mechanical Engineering Department at the University of Delaware for providing me with an excellent undergraduate education.
- Thank you to Shelley Crawford and fellow SAI sisters who have kept in touch through the years. Thank you for your friendship and support.

Table of Contents

List of Tables

List of Figures

Chapter 1: Introduction

There is very little literature available on the detailed high cycle vibration testing results for lead-free (a.k.a. Pb-free) solders. As lead-free solders are used more frequently in electronic products, it is important to understand how they compare to conventional tin-lead (a.k.a. SnPb) solders that companies are used to using. The purpose of this work is to give detailed testing results which will provide guidance to users who have to make the switch to lead-free solders.

This paper describes the accelerated harmonic testing of plastic ball grid array (PBGA) components and leadless chip resistors (LCRs) mounted to test coupons. A test method was developed and first validated for collecting trustworthy data. Then ball grid arrays and LCRs attached to printed wiring boards (PWBs) were tested and failure data was collected. Weibull plots and Basquin relations were generated for each solder and compared, and destructive analysis was done to determine any differences in crack propagation.

First, current literature on fatigue of Pb-free solders will be explored. The following chapter will describe the testing and analysis of the BGAs, which were attached to PWBs with either standard eutectic SnPb solder or tin-silver-copper (SAC) solder (specifically, SAC305). After presenting the BGA tests, testing of the LCRs, which were attached to PWBs with SnPb solder, SAC solder (specifically, SAC305 and SAC105) , and tin-nickel-copper solder (specifically, SN100C), will be discussed.

Chapter 2: Literature Review

There have been some vibration testing and analyses done on different Pb-free solders, but further study is needed. The key point is as Osterman and Dasgupta noted [3], there are inconsistencies in the current literature on the lifetime of Pb-free solders as compared to conventional SnPb solder. Some of the relevant work is very briefly noted here.

Wong et al. performed harmonic testing on BGAs attached to a FR-4 board using SnPb and SAC solders [21]. The test setup consisted of an FR-4 board with one ball grid array placed in the center. 45 test boards with SAC BGAs and 31 test boards with SnPb BGAs were tested under harmonic vibration of acceleration input levels ranging from 0.75 g to 4 g at the natural frequency of the board. The time of the BGA failure was determined when the monitored electrical resistance of a circuit formed with the BGA solder interconnects increased by 100%. Strain of the PWB was recorded during these tests. Cyclic bend and cyclic shock tests were also performed. A durability curve of board strain versus time to failure was created from the data collected from all of the tests, and the results show that the durability of the BGAs attached with the two solders crossed over in the range of one hundred to one thousand cycles. After one thousand cycles, SAC performed better than the SnPb-attached BGAs. SnPb performed better than SAC before one hundred cycles. Destructive analysis was performed, and this analysis showed that most failures resulted from cracks initiating in and propagating through the

bulk solder in a diagonal pattern. A handful of failures were from cracks in the inter-metallic compound.

Zhou, Al-Bassyiouni, and Dasgupta performed harmonic tests of resistors and BGAs, and their results were opposite to that of Wong's [5]. Resistors and BGAs were attached to FR-4 PWBs with eutectic SnPb and SAC305 solder. The boards were tested at the first resonant frequency of the PWB (169Hz) at acceleration levels of 9 g, 10.5 g, and 12 g. Their tests showed that SAC305 outperformed SnPb in the region, under ten million cycles, while SnPb outperformed SAC305 in the region over ten million cycles.

Lee performed random vibration tests on PBGAs attached to PWBs with 95.5Sn-3.9Ag-0.6Cu solder and conventional eutectic SnPb solder in two different sizes (27x27mm and 35x35mm) [20]. An increase in resistance of 100Ω was considered a failure of the PBGA. Frequencies in the random test occurred between 20 Hz and 2000 Hz, and the testing time lasted 6 hours. Test boards were mounted in a rack tower which was secured on the shaker. The peak-to-peak maximum load was no more than 6 g. No failures were observed from this testing, which indicates that these testing conditions have little to no effect on the BGA solder joints. Three-point bend tests were also performed and showed that smaller package sizes performed better under the testing.

Tzan and Chu examined chip scale packages attached with eutectic solder and Sn3.5Ag solder, to PWBs with two different finishes – gold over nickel and organic solderability preservative (OSP) [19]. Harmonic vibration, three-point bend and pull tests were performed. The harmonic vibration test was performed with a peak acceleration of 20 g and a sweep of frequencies ranging from 20 Hz to 2000 Hz. There

were no failures from this test. The pull tests showed that the tin-silver solder with the nickel-gold board finish required the most force to pull off the package. The three-point bend test showed no significant differences in the two solders or the two board finishes.

Barry et al developed a test to subject eutectic SnPb, SAC305, and SN100C solders to high cycle fatigue [15]. This test did not include components attached to a PWB with solder, but solder connected two rods. The solder connection size resembled the size of a solder connection of components to a PWB. Eight solder interconnects were tested at a time, at a frequency of 600Hz, until all specimens had failed. Acceleration of the rods ranged between 20 g and 50 g. The results of this test showed that SnPb performed best at high cycle fatigue, with SN100C performing the poorest and SAC305 performing in between.

The Joint Council on Aging Aircraft (JCAA) and Joint Group on Pollution Prevention (JG-PP) devised and tested electronic components attached to PWBs with SnPb and Pb-free solders, and compared results to predictions of CirVibe Inc.'s *CirVibe* software, which predicts component lifetimes [18]. The tests were performed by Boeing Phantom Works. Tested components include ceramic leadless chip carriers, plastic leaded chip carriers, thin small-outline packages (TSOPs), thin quad flat packs (TQFPs), BGAs and plastic dual in-line packages (PDIPs). The test setup included boards that were manufactured with Pb-free solder, and boards that were made to simulate a board that was originally manufactured with SnPb solder and re-worked with Pb-free solder. An increase in resistance to 300Ω was considered a failure. Boards were step stress tested from load levels of 9.9 g to 20 g in x,y, and z directions. Results showed

reasonable agreement between test data and predictions made by the software. These predictions were then used to compare the SnPb and SAC305 solders that attached the BGAs to the test PWB's. These predictions showed that the SnPb solder lifetime is much longer than that of the SAC305 lifetime.

Lim et al. examined the reliability of 256 I/O PBGAs when put through accelerated harmonic vibration excitations until failure [12]. Wang et al. tested chip scale packages for 2 hours using guidelines for automotive tests, and all components passed this test - no component was tested to failure in their vibration testing [10]. Song et al. examined the effects of high silver (a.k.a Ag) content in Pb-free solder, and found that the addition of Ag can actually increase damping properties, thus increasing time to failure [9]. This work was on bulk solder and not component attaches. Tu and Chan looked at how intermetallic compounds in a solder can impact the lifetime of that solder using a torque machine setup [8].

In summary and as pointed out earlier in the introduction, there is no consensus on the difference in high cycle fatigue durability between component attaches with SnPb solder and Pb-free solder. This paper reports on the high cycle fatigue durability testing of two different electronic components. The first set of durability tests were on BGAs attached to PWB test coupons with eutectic 63/37 SnPb and SAC305. The second set of tests were LCRs attached to PWB test coupons with eutectic 63/37 SnPb, SAC305, SAC105, and SN100C.

Chapter 3: Harmonic Vibration Testing of 160 I/O PBGA Soldered to PWB with SAC305 and Eutectic PbSn Solder

This chapter describes the testing done to generate high cycle fatigue failures in BGAs attached to PWBs with standard eutectic PbSn solder and tin-silver-copper SAC305 solder and discusses the test results. The following text is from a paper in process for publication.

3.1 Test Setup

Vibration tests of solder interconnects were conducted in a vibration shaker setup, shown in Figure 1, consisting of a Data Physics *SignalStar* controller hooked to a Data Physics *Signal Force* amplifier and shaker. Two independent computers were used for data acquisition. One computer logged the PWB strain using an A/D card and National Instruments' *Lab VIEW* software. The other computer logged the daisy-chained resistances in each PBGA using the Agilent Technology's *Benchmark Data Logger* software. The shaker setup consists of the shaker, mounting plate, fixture base, and clamps, as depicted in Figure 2.

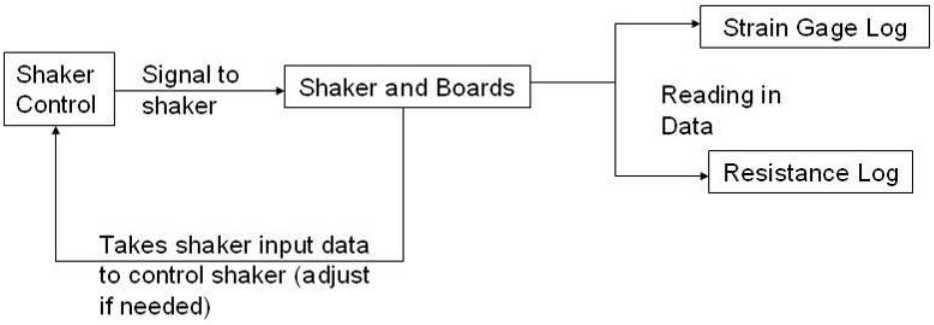

Figure 1. Vibration Test Setup

Figure 2. Shaker

The mounting plate fixture can hold two test boards at a time. For this test, the test specimens consisted of PWBs with eight daisy-chained partial array 160 I/O, 0.8 mm pitch Amkor BGAs. Each BGA contained a dummy silicon die and were internally routed so a daisy chain circuit could be employed to detect ball attach failures. Figure 3 below is a schematic of the Amkor ball grid array and Figure 4 shows the layout of the eight components on the test coupon board. The test coupon PWB was 1.6 mm thick Polyclad 370HR with an immersion silver (ImAg) finish. The test boards were assembled by

Benchmark Electronics using standard reflow profiles for the two solders. Before testing, the boards were preconditioned and artificially aged by subjecting them to 100°C for 24 hours. After preconditioning the boards were immediately wired and setup for testing. The time between the end of preconditioning and beginning of testing on average was 24 hours. Testing temperatures varied from 21° C to 32° C due to the laboratory not being air conditioned. While there are eight BGAs attached to the test coupon board, tests were time terminated after the four center region BGAs were found to failure. All reported failure data is from these four BGAs.

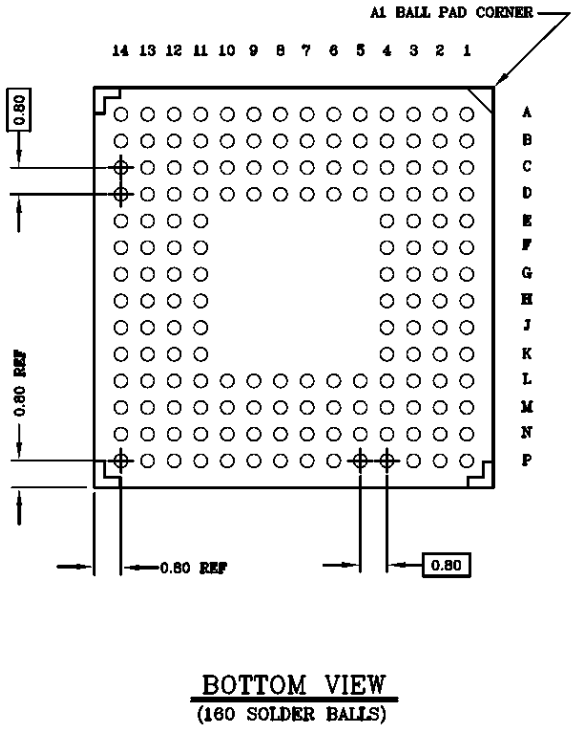

Figure 3. Amkor BGA Schematic

The test boards are consistently positioned in the shaker fixture using a plated through-hole in the corner of the boards. Figure 4 shows the test boards mounted in the shaker fixture. The boards are clamped down on the shorter-length edges with a bar and grade 5

steel bolts. Double-sided tape is placed between the boards and the clamping bar to prevent potential walking of the board. This tape did provide some additional damping, but was consistently used in all testing. The clamping bolts were then tightened in a diagonal pattern, first to 8 ft-lbs and then to 16 ft-lbs. An effort was made to insure fixture consistency in all testing. Figure 4 also shows the order of bolt tightening.

Note that the groupings of BGAs are not exactly centered between the two clamps. The BGA locations were measured from the clamped edge location and centered based on these measurements with the intent that the BGA locations on each side of the board will be the same distance from the centerline. However, the BGA locations were measured with a simple ruler, and boards were centered by marked locations measured by the ruler, instead of a more precise measuring procedure, for instance laser measurements. As a result, there was an error of approximately +/-5mm – this is a small amount, but still made a big difference – as a result, two of the four outer BGAs never failed because they were a few millimeters farther away from the centerline. This means that the BGAs see slightly different loading based upon their distances from the clamped edges. This is why board strain is carefully measured for each BGA.

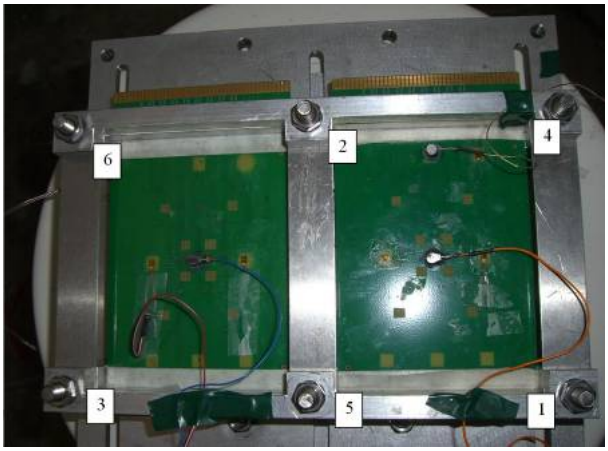

Figure 4. Board Setup

Strain data is captured at 5,000 Hz during a one-second capture period. This one-second capture is repeated every five minutes. Naturally the strain gages and recording circuits are carefully calibrated before every test.

Resistance data is collected every 10 seconds during the testing using Agilent Technology software and data cards. An initial resistance data file is recorded prior to each test. This initial data file has at least 40 points of data. These data points are averaged to give an initial resistance value prior to the test. A failure is defined as a 20% increase in resistance from the initial average resistance value

Accelerometers were placed on the test boards. These were sometimes placed between the center PBGA components and the outer components, at 1/4 of the clamped longitudinal length of the board, in the latitudinal center. At other times, the accelerometers were placed alongside the center components, at 1/2 of the clamped longitudinal length of the board, off the latitudinal center. Figure 5 shows these accelerometer positions. Three accelerometers were used during each test. One accelerometer (PCB Piezotronics brand) screws in to the shaker base. This accelerometer

response was the control accelerometer for the *Signal-Force* software. Two more shear accelerometers (one Dytran and one PCB Piezotronics) were used,one accelerometer per board. The calibration of each accelerometer was certified by the manufacturer.

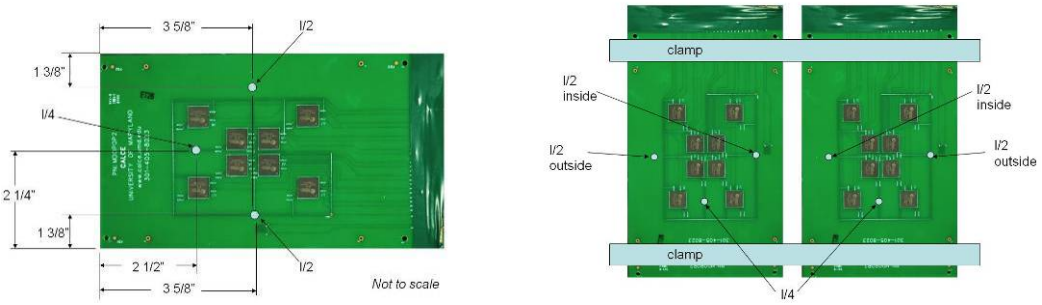

Figure 5. Accelerometer Locations

3.2 Repeatability Tests

To make sure that the vibration tests would give consistent results, several tests were conducted to simulate different testing scenarios. Transmissibility and strain of the board was monitored during these tests to check repeatability and consistency. Three scenarios were tested:

1. The first scenario was a short vibration test – starting a test and stopping it in a short amount of time, and repeating several times. The shaker was powered on and started up for about one minute, and stopped for one minute. This was repeated several times.
2. The second scenario was a longer version of the first test. The shaker was powered on and the test was run for 5 to10 minutes, and then turned off for 10 minutes, and repeated.

3. The third scenario was to clamp and unclamp the fixture – the board was taken out of the fixture, and then placed back onto the fixture, and tightened back in. Then the shaker ran for five minutes, and then stopped. This procedure was repeated several times.

After running these tests and analyzing the data, it was confirmed there were no changes in accelerations or strains due to the stopping, restarting and clamping/unclamping of the boards. These results gave us more confidence in the consistency of the test setup and vibration level from one testing sample to the next.

3.3 Board Characterization

Initial testing was done to characterize the boards. The test started with a frequency sweep from 50 Hz to 300 Hz at load levels of 1 g, 3 g, 5 g, 7 g, and 10 g shaker inputs. The natural frequencies of the boards were found to be in the range of 197 Hz to 208 Hz. Strain data was initially recorded directly underneath all eight BGA components. The initial strain mapping tests showed that the BGAs on each side of the longitudinal center line experienced the same amount of strain, so one gage per different distance from the clamped edge of the board was deemed to be enough. All gages were oriented along the longitudinal axis of the board, in the direction of maximum board flexure. The stiffness of the BGAs will be addressed in Chapter 5, when the data is compared to other strain data which was measured away from the component. The shaker was controlled by the base plate acceleration. This acceleration controlled the board acceleration level and therefore the strain and times to failure of the BGA packages.

To determine an appropriate high load and low load harmonic excitation, pre-test boards were subjected to a base excitation of 1 g, 3 g, 5 g, 7 g, and 10 g near their natural frequency. Testing was conducted as close to the natural frequency as possible to generate the maximum board strain. Resistance and strains were recorded during all testing. Based on the time to failure of the BGAs on the boards, it was determined that base excitations of 3 g and 5 g would be an appropriate high and low load level.

3.4 Testing

Once the frequency was confirmed, the testing took between 2 and 4 hours for the central grouping of four BGAs to fail at the high harmonic excitation level and between 6 and 30 hours for the low harmonic excitation level. Strain and resistance data were collected during each test, and acceleration plots generated from the Data Physics *SignalCalc* software every few hours. Table 1 shows the average board acceleration and board strain range for both the high and low vibration excitation level, directly under one of the center four BGAs. These values are average or typical values because the central four BGA grouping is not exactly centered between the clamped edges and each test board reacted slightly differently to the base excitation. Maximum PWB strain rates ranged between 1.1×10^{-1} and 2.7×10^{-1} per second which is at least two to three orders of magnitude faster than thermal cycling tests [25]. The strain rate is calculated by multiplying the strain range by twice the frequency.

Base Excitation Level	Board Acceleration	PWB Strain Range
Low – 3 g	135 g	2.8E-4
High – 5 g	165 g	6.3E-4

Table 1. **Average BGA PWB Strain Ranges**

3.5 Results and Analysis

Figure 6 is a compilation of all the failure data and is a durability plot. The horizontal axis is the number of vibration cycles until the daisy-chained BGA failed. (Remember that failure is defined as an increase in the daisy chain circuit electrical resistance of 20%.) The number of cycles is computed by multiplying the time until failure by the vibration excitation frequency. The vertical axis is the board strain range as measured by the strain gage directly under the BGA of interest. Each square in the plot represents the failure of a BGA attached to the board with 63/37 SnPb solder. There are 37 failure points for the SnPb solder. The 37 diamonds are failures of BGAs attached to the board with SAC305 solder. These failure sets include the data obtained during the early board characterization testing which determined an appropriate high cycle fatigue testing excitation level.

Looking at just the data points, or data clouds, of each solder type, there appears to be little difference between the two solders. A power law regression (linear regression in log-log space) was conducted on the two failure data sets. The two regression lines are plotted in Figure 6 and are overlapping. The coefficient of determination (r^2) is only about 0.6 for both cases and the uncertainty in the power law coefficients is much greater

than the differences in their values between the two solders. Regression analysis was performed on the two regressions shown in Figure 6. It was found that the confidence levels of the regression coefficients and exponents overlapped each other as shown in Table 2 and Table 3. The mean regression coefficient of SnPb lies between the upper and lower 95% confidence intervals of the SAC305 coefficient, and the mean regression coefficient of SAC305 lies between the upper and lower 95% confidence intervals of the SnPb coefficient. The same is true for the exponents of the two solders. The regression fit and analysis shows that there is no statistical difference between the two failure sets.

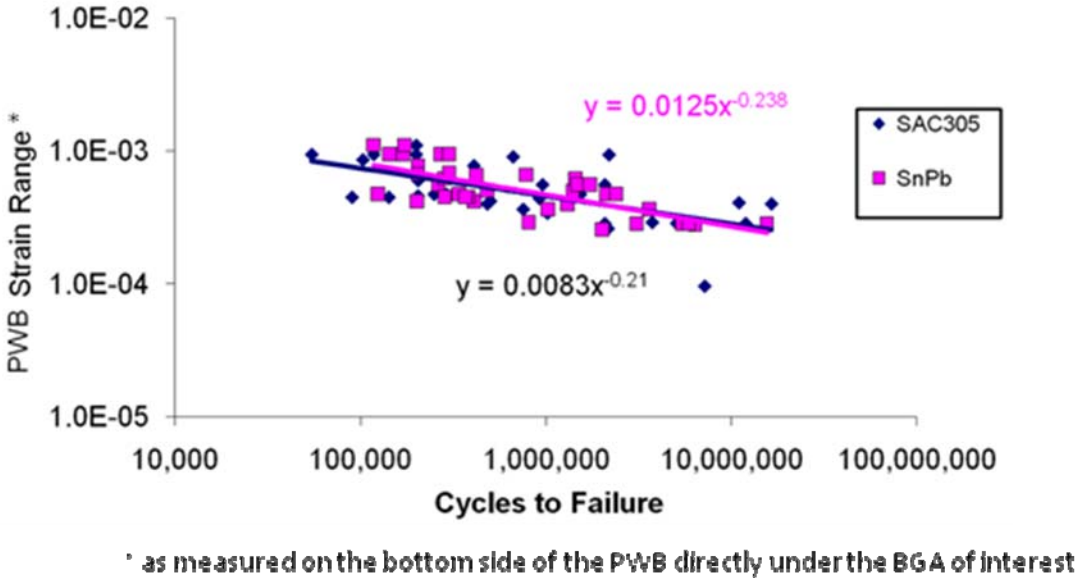

Figure 6. Durability regressions for SnPb and SAC305 solder balls under harmonic vibration

SnPb Regession Analysis

	Mean	Upper 95%	Lower 95%
Coefficient	0.0125	0.0350	0.00450
Exponent	-0.238	-0.162	-0.314

Table 2. Analysis of SnPb BGA durability regression

SAC305 Regression Analysis

	Mean	Upper 95%	Lower 95%
Coefficient	0.00834	0.0266	0.00261
Exponent	-0.210	-0.124	-0.296

Table 3. Analysis of SAC305 BGA durability regression

The one trend that is naturally expected is that the number of cycles to failure will increase with a decrease in board strain range. This trend is seen in the data cloud as well as the negative slope in the power law regression lines. The Basquin high cycle fatigue relation,

$$\sigma^b N_f = \text{constant} \qquad \text{or} \qquad N_f = (\text{constant})\ \sigma^{-1/b}$$

where N_f is the cycles to failure and σ is the stress (which is directly proportional to the board strain range), tells us that the solder fatigue exponent, b, is the negative inverse of the power law exponent in the regression equation. The fatigue exponent for the SAC305 regression is 4.20 and the fatigue exponent for the SnPb is 4.76. CALCE recommends a solder fatigue exponent of 6.4 for long life field conditions [22], but recognizes that this can drop to as low as 4 under accelerated test conditions [22]. Therefore, these fatigue exponents are consistent with accelerated test conditions.

3.6 Failure Analysis

BGAs that failed were cross-sectioned to identify and compare the locations of failures. Cross sections were taken for parts that exhibited early failures and late failures for both SnPb and SAC305 components. As seen in

Figure 7, cracks were generally found to be through the solder balls, near the component-side of the solder.

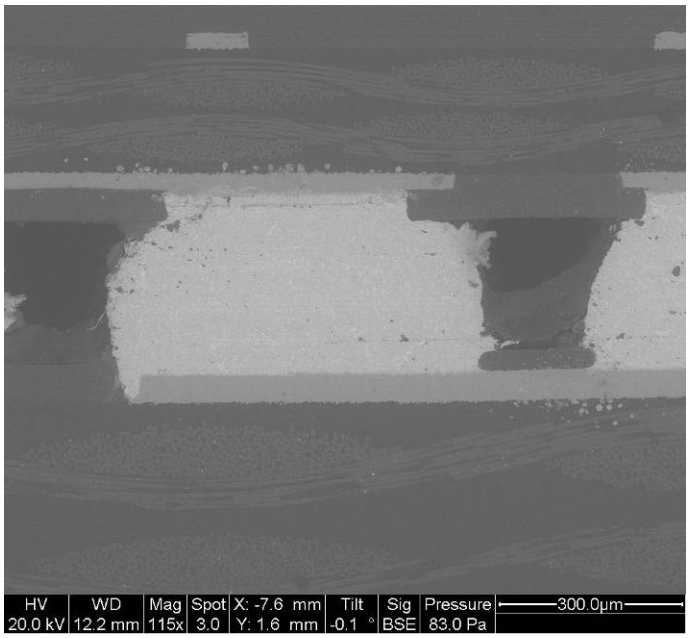

Figure 7a – Solder crack of SnPb

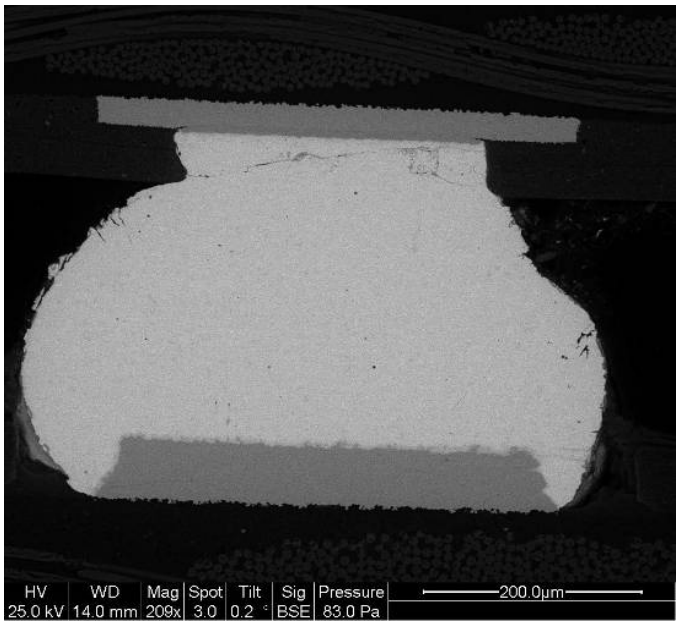

Figure 7b – Solder crack of SAC305

Figure 7. Solder ball crack comparison

3.7 Conclusion

Harmonic vibration testing was conducted in room ambient conditions similar to outdoor temperatures (21-32° C) on BGA tests assemblies with either SnPb or SAC305 solder attachments. The test frequency was set near the test assembly natural frequency to accelerate the testing and generate high cycle fatigue failures in a reasonable period of time. During testing the board strain directly under the BGAs and the electrical resistance of circuits that include the BGA solder interconnects were monitored. A 20% increase in the daisy chain circuit resistance was deemed to be failure. A durability plot was created of vibration cycles to failure versus monitored coupon board strain directly under the BGA. The final failure data included results from 37 SnPb soldered BGAs and 37 SAC305 soldered BGAs. The data included failures that occurred just under 100,000 cycles to just over 10,000,000 cycles. No significant difference in the durability was noted between the two different solders.

Chapter 4: Harmonic Vibration Testing of LCRs Soldered to PWB with Pb-free and Eutectic SnPb Solder

This chapter discusses harmonic vibration testing of LCRs attached to PWBs with standard eutectic SnPb solder, tin-silver-copper solders SAC105 and SAC305, and tin-nickel-copper (SN100C) solder. The following text is from a paper in process for publication.

4.1 Test Setup

The vibration shaker setup shown in Figure 8 consists of a Data Physics *SignalStar* controller hooked to a Data Physics *Signal Force* amplifier and shaker. Two independent computers were used for data acquisition. One computer logged the PWB strain measured using strain gages and an A/D card connected to National Instruments' *Lab VIEW* software. The other computer logged the daisy-chained resistances in each chip resistor using Agilent Technology's *Benchmark Data Logger* software. Figure 8 shows a schematic of the setup. The shaker setup consists of the shaker, mounting plate, fixture base, and clamps. Figure 9 shows this setup.

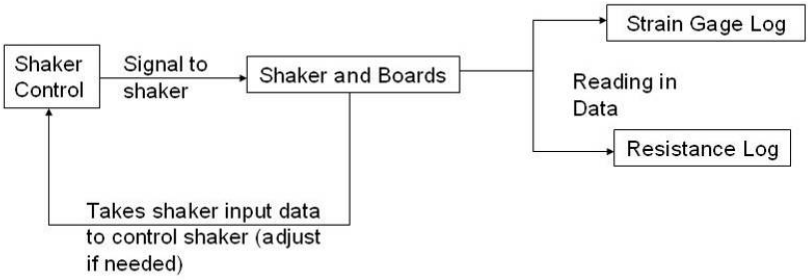

Figure 8. Vibration Test Setup

Figure 9. Shaker Assembly

The mounting plate fixture can hold two test boards at a time. However for this testing, only one resistor board was tested at a time. To preserve symmetry, test board of similar dimension but with no mounted parts was placed in the second board position. Each resistor board had forty 2512 LCRs from Practical Component. The resistors are zero-ohm resistors. Each resistor board was designed with two pad sizes, which will be referred to as standard or narrow. The standard pad dimensions were 3.3 x 1.65 mm. The narrow pad dimensions were 0.66 x 1.65 mm. There were twenty resistor positions with narrow pads and twenty resistor positions with standard pads on each resistor board. Figure 10 shows the resistors mounted to standard pad and narrow pad positions. For each resistor board, resistor positions were formed in five columns with eight positions

per column, as shown in Figure 11. The PWB was 1.6 mm thick Polyclad 370HR with an electroless nickel immersion gold (ENIG) pad finish. The test boards were fabricated by DDi Global and assembled by Benchmark Electronics using standard reflow profiles for the four different solders. Before testing, the boards were preconditioned and artificially aged by subjecting them to a temperature of 100° C for 24 hours. After preconditioning, the boards were immediately wired and setup for testing. The time between the end of preconditioning and beginning of testing on average was 24 hours. Testing temperatures varied with the outdoor temperatures, which ranged from 10 °C to 32 °C due to the laboratory not being air conditioned or heated. Even though there are 40 resistors attached to the test coupon board, due to the higher central region board strain the central three columns of resistors were the only columns to show failures. All reported failure data is from resistors positioned on the three central columns.

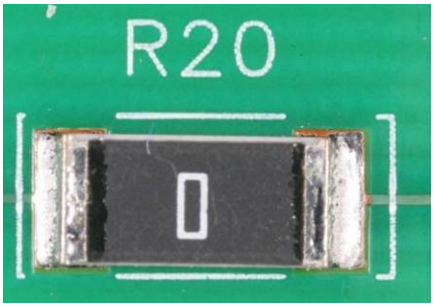

Figure 10a – Standard pad position

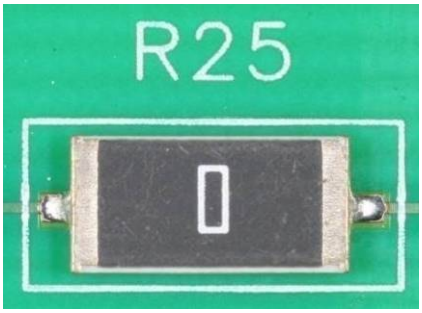

Figure 10b – Narrow pad position

Figure 10. 2512 Resistors Attached to Standard Pads and Narrow Pads

The test boards are consistently positioned in the shaker fixture using a locating plated through-hole in the corner of the boards. Figure 13 shows one half of the fixture and one mounted test board. The boards are clamped down on the shorter-length edges with a bar and grade 5 steel bolts. Double sided tape is placed between the boards and the

clamping bar to prevent potential walking of the board. This tape did provide some additional damping, but was consistently used in all testing. The clamping bolts are then tightened in the same diagonal pattern, first to 8 ft-lbs and then to 16 ft-lbs. A special effort was made to insure fixture consistency in all testing.

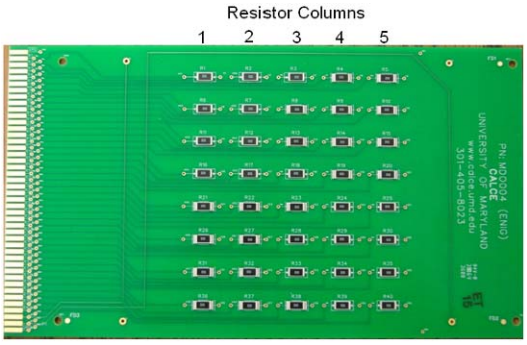

Figure 11. Resistor Board Layout

The board strain data is captured at 5,000 Hz during a one-second capture period. This one-second capture is repeated every five minutes. All strain gages & recording circuits are carefully calibrated before every test.

Resistance data is collected every 10 to 50 seconds during the testing using Agilent Technology software and data cards. An initial resistance data file is recorded prior to each test. This initial data file has at least 40 points of data. These data points are averaged to give an initial resistance value prior to the test. A failure is then considered to be a 20% increase in resistance from the initial average resistance value

Accelerometers were placed on the test boards. These were always placed in the center of the middle column of resistors, one directly under resistor 8 and one directly under resistor 33, as shown in Figure 12. The stiffness of the resistors will be addressed

in Chapter 5, when the data is compared to other strain data which was measured away from the component. Two accelerometers were used during each test. One accelerometer (PCB Piezotronics brand) screws in to the shaker base and is the control accelerometer for the Data Physics *Signal-Force* shaker software. The other accelerometer (also PCB Piezotronics brand) was placed on the test board. The calibration of each accelerometer was certified by the manufacturer.

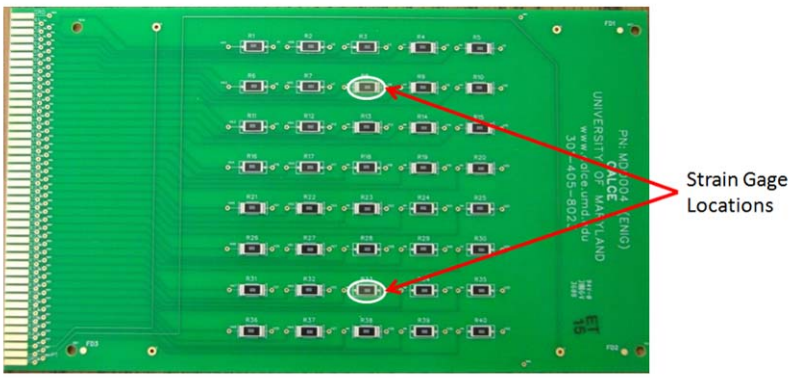

Figure 12. Strain Gage Locations on Resistor Board

4.2 Repeatability Tests

To make sure that the vibration tests would give consistent results, several tests were conducted to simulate different testing scenarios. Transmissibility and strain of the board was monitored during these tests to check repeatability and consistency. Three scenarios were tested:

1. The first scenario was a short vibration test – starting a test and stopping it in a short amount of time. The shaker was powered on and started up for about one minute, and stopped for one minute. This was repeated several times.

2. The second scenario was a longer version of the first test. The shaker was powered on and the test was run for 5 to 10 minutes, then turned off for 10 minutes, and repeated.
3. The third scenario was to clamp and unclamp the fixture – the board was taken out of the fixture, and then placed back onto the fixture, and tightened back in. Then the shaker ran for 5 minutes, and then stopped. This procedure was repeated several times.

After running these tests and analyzing at the data, it was confirmed there were no changes in accelerations or strains due to stopping and restarting or clamping and unclamping of the boards. This gave us more confidence in the consistency of the test setup and vibration level from one testing sample to the next.

4.3 Board Characterization

Initial testing was done to characterize the boards. The test started with a sweep from 50 Hz to 300 Hz. The natural frequency of the boards was found to be in the range of 202 Hz to 212 Hz.

The groupings of resistors are not exactly centered between the two clamps. This is best seen in Figure 13. This means that the resistors see slightly different loading based upon their distances from the clamped edges, or the true centerline of the board. Figure 14 is a plot of measured strain at the various column locations versus the theoretical response for a perfectly clamped board. Also in the figure is the response from a board that is not perfectly clamped. This line better matches the measured strain. Not having perfectly clamped boundary conditions is expected because one almost always has

some torsional compliance in the clamping. This exercise did give us confidence in the strain readings at the various column positions.

Initially, strain data was recorded directly underneath the outermost resistor columns and the center resistor column. In later testing, strain gages were only placed underneath the center resistor column and the strain at the other column locations was calculated using the curve in Figure 14.

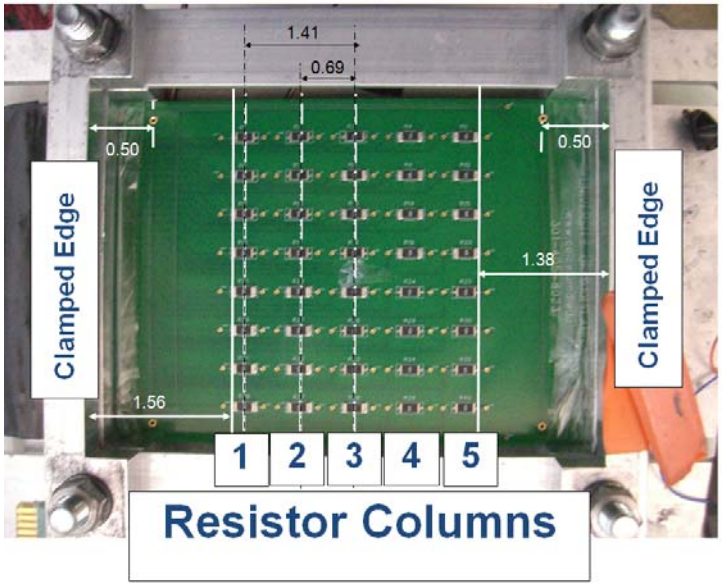

Figure 13. Single Test Board Mounted on one Side of Fixture

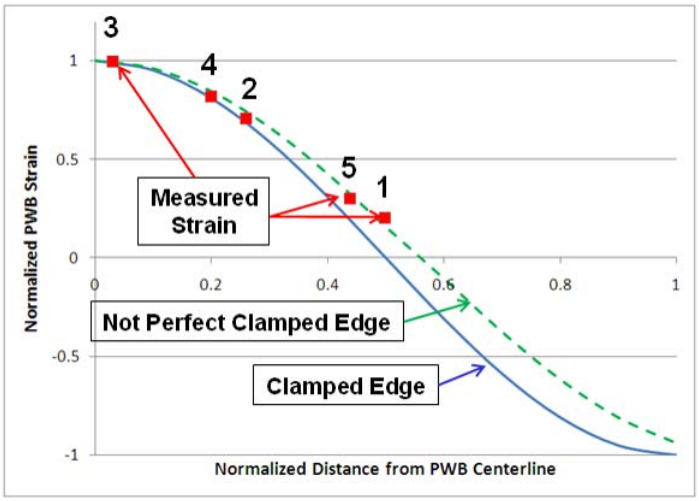

Figure 14. Strain as a function of column location

All gages were oriented along the longitudinal length of the board, in the direction of maximum board flexure. Originally, the shaker was controlled by the shaker base acceleration, but later it was controlled by the measured board acceleration. Using this method of control kept the acceleration level more constant over long test times.

4.4 Testing

Boards were tested at different low harmonic excitation levels near their natural frequencies. Testing was generally terminated, after at least 100,000,000 cycles which corresponds to minimally one week of continuous testing. First failures occurred between 100,000 cycles and 600,000 cycles depending on solder and pad type. Failures were carefully logged throughout the test by monitoring the circuit resistances of the resistors under test. Besides circuit resistances, strain data were continually collected. In addition, acceleration plots were generated from the Data Physics software every 24 hours. Table 4 shows a typical board vibration excitation level and the corresponding board strain range for each column of resistors. These values are typical values because each

test board reacted slightly differently and the tests were conducted at different excitation levels - The strain ranges of the center column of resistors ranged from 524 to 645 microstrain for board excitations of 110G. One test yielded a strain range of 980 microstrain from a board excitation of 130G. Maximum PWB strain rates were on the order of 2.7 x 10^{-1} per second which is at least two to three orders of magnitude faster than thermal cycling tests [25]. The strain rate is calculated by multiplying the strain range by twice the frequency.

	Average Strain Ranges(μs)				
Board Excitation (g)	Col 1	Col 2	Col 3	Col 4	Col 5
110	122	415	603	490	187
125	128	433	628	511	195
130	200	680	988	803	307

Table 4. Average Strain Ranges for LCR PWB

4.5 Results and Analysis

Figure 15 provides two durability plots with resistor failure data. Figure 15a is the plot for the narrow pad failures and Figure 15b is the plot for the standard pad failures. Each plot presents failures in a board strain range/cycle to failure space. The number of cycles is computed by multiplying the time until failure by the vibration excitation frequency. The vertical axis is the board strain range as measured by the strain gage directly under the resistor column of interest. The two failure distributions are not shown on a single plot since for a given amount of PWB strain, the stresses are different in the two pad configurations. The narrow pad solder joints obviously sees a higher solder stress than the standard pad solder joints since the pads are 1/5th the size. There are 24 failure points for the SnPb solder with narrow pads, shown as purple squares in Figure

15a. The 31 green triangles in Figure 15a are failures of resistors attached to the board with narrow pads of SAC305 solder. The 12 blue triangles in Figure 15a represent failures of resistors that were attached to the board with SN100C solder, and the orange diamonds represent failures of resistors that were attached to the board with SAC105 solder. Standard pad failures are shown in Figure 15b and are represented by the pink squares for SAC105, yellow circles for SnPb, green squares for SN100C and red circles for SAC305. The standard pad failures are from time terminated tests. Testing was generally stopped at 100 million cycles or sooner, regardless of the number of failures, due to time limitations on completing all the tests.

The one overall data trend that is expected is that the number of cycles to failure will increase with a decrease in board strain range. This is generally seen in the data cloud as for each solder type. The Basquin high cycle fatigue relation,

$$\sigma^b N_f = \text{constant} \qquad \text{or} \qquad N_f = (\text{constant})\ \sigma^{-1/b}$$

where N_f is the cycles to failure and σ is the stress which is directly proportional to the board strain range, tells us that the solder fatigue exponent, b, is the negative inverse of the power law exponent in the regression equation. A power law regression (linear regression in log-log space) was attempted on each solder type, but the coefficient of determination (r^2) was small enough, less than 0.4, that it was improper to rely upon a regression fit. The uncertainty in the power law coefficients is just too large, but the overall expected trend in the data is seen.

Just visually looking at the data points, or data cloud, for the narrow pad resistors in Figure 14a there appears to be little difference between the eutectic SnPb and the SAC305 solder. The SN100C and the SAC105, dark blue triangles and orange diamonds, definitely fail before both the SnPb and the SAC305. These findings are the same for the standard pad failures presented in Figure 15b. There are fewer failure points for the standard pad resistors because the test was typically terminated at 100,000,000 cycles before many of the standard pad resistors had failed. Even then, it can be clearly seen that the SN100C and the SAC105 fail before the SAC305 and SnPb. There were only two SnPb standard pad resistor failures, and they appear to last longer than the SAC305. This is just an observation and cannot be any stronger due to lack of failure data at an extreme number of cycles.

It is recognized that the failure data is very scattered. At any particular board strain range, the range in cycles to failure for resistors seeing the same strain range varied by an order of magnitude or more. Weibull plots of the failure distributions were attempted, as seen in Appendix D, but due to the availability at most four data points, resistors with the same type of pad size in a test board column, the plots made little sense. The effective Weibull slopes were less than one and sometimes appeared to show two different failure distributions, one of early failures and one for late failures. With only four data points these results were inconclusive.

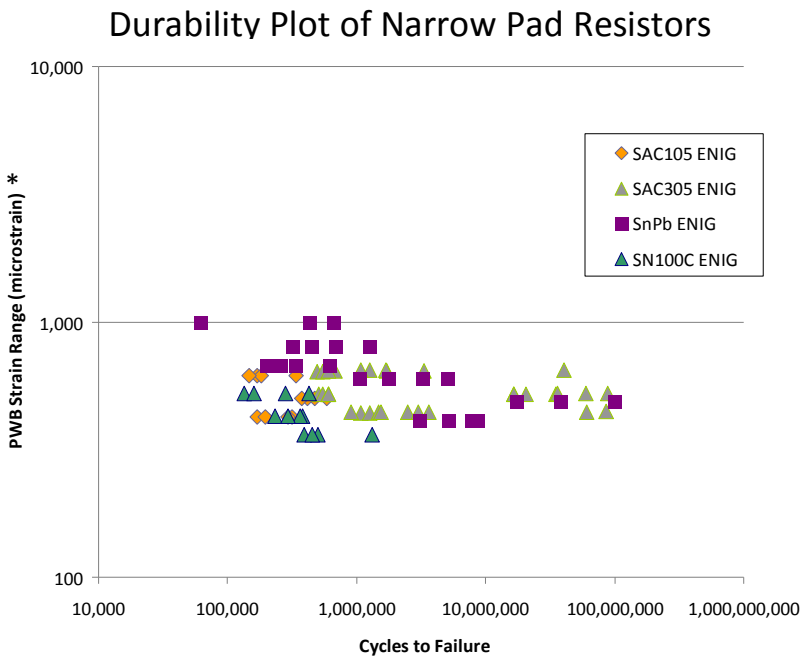

* as measured on the bottom side of the PWB directly under a resistor in the column of interest

Figure 15a. Durability Plot of Narrow Pad Failures

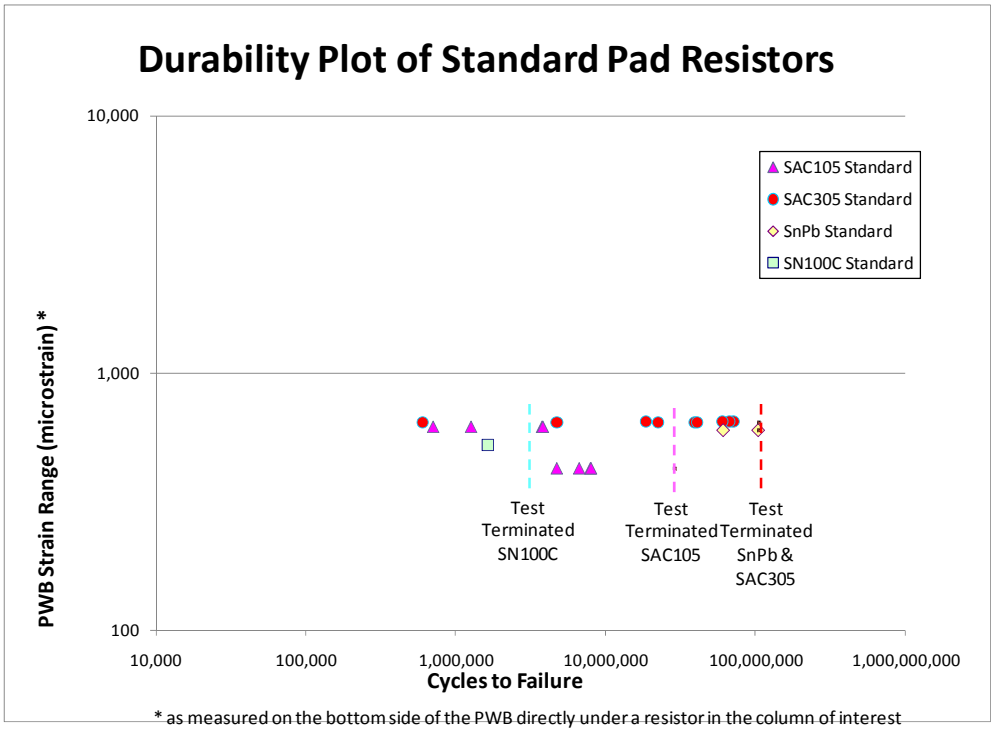

* as measured on the bottom side of the PWB directly under a resistor in the column of interest

Figure 15b. Durability Plot of Standard Pad Failures

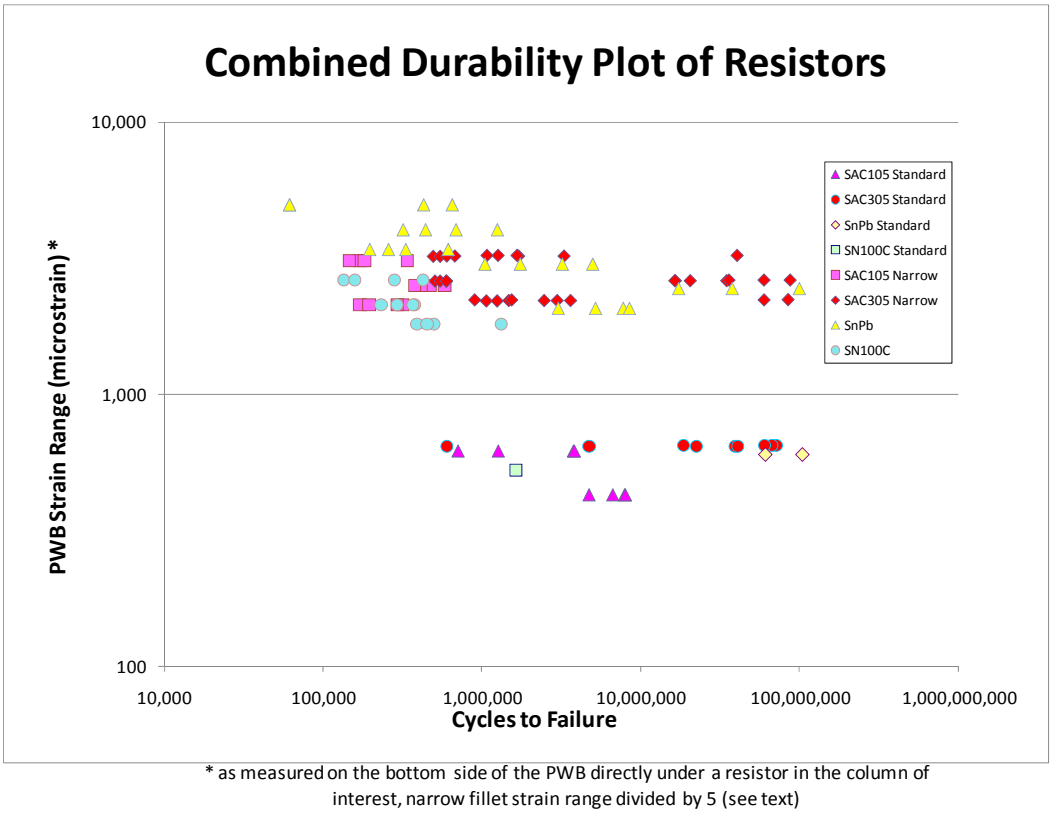

Figure 15c. Combined adjusted durability plot of narrow and standard pad resistors

Figure 15. Durability plots for LCR solders

Attempts were made to correlate the narrow pad resistors with the standard pad resistor results. The narrow pad resistors were 1/5 the size of the standard pad resistors, see Figure 10. There was approximately 1/5 the solder attaching the resistor to the board as with the standard pad. Thus for a first approximation, for the same amount board strain or curvature, the solder in the narrow pad resistor saw 5 times the stress as the standard pad resistor. This is consistent with the fact that the narrow pad resistors generally failed before the standard pad resistors. In Figure 15c, the failure data for both the narrow and standard pad resistors are plotted together on the same durability plot, where the PWB strain range is multiplied by 5 for the narrow pad resistors. If the approximation is correct that the narrow pad resistors fillets see 5 times the stress of the standard pad resistors, by

multiplying the PWB strain range for the narrow pad resistors by 5 it should result in the same stress in the solder fillet as would be seen by a standard pad resistor. By viewing the results shown in Figure 15c, there is an obvious problem because the failure groupings for the two pad sizes are widely separated. The simple correction factor based upon pad size is wrong and a more sophisticated three dimensional stress analysis must be done. A 3D stress analysis between the two resistor pad sizes is beyond the scope of this thesis.

The data does show that there is very little difference in durability between the SAC305 and SnPb solders. Both SN100C and SAC105 solder are not as durable and SnPb or SAC305 under the tested conditions. It is not demonstrated with our data, but some have indicated that up to one million cycles to failure, the SAC305 solder shows a slightly better durability. Our data does possibly support the other observation that has been made by others that after one million cycles, the SnPb solder then performs slightly better [5].

4.6 Failure Analysis

Resistors that failed were cross-sectioned to identify and compare the locations of failures. Cross sections were taken of resistor interconnects which experienced early and late failures for all four solder types with the hopes of an explanation for the extreme ranges in cycles to failure. As seen in Appendix E, cracks were generally found to be through the solder, starting under the resistor at the inner land and continuing until it reaches the pad. Once it reaches the pad it generally takes the shortest path to the outside.

No significant difference of crack path was observed between early and late failures or solder type.

4.7 Conclusion

Zero ohm 2512 LCRs were attached to a PWB test coupon with standard and narrow pads (narrow pads were 1/5 of the standard pad width). Solders used were conventional eutectic 63/37 tin-lead solder, tin-silver-copper solders, SAC305 and SAC105, and tin-nickel-copper solder, SN100C. Harmonic vibration testing was conducted on the populated test vehicles near the coupon's natural frequency to accelerate the testing and generate high cycle solder attach fatigue failures in a reasonable period of time. Maximum PWB strain rates were on the order of 2.7×10^{-1} per second which is at least two to three orders of magnitude faster than thermal cycling tests [25]. During testing the coupon board strain directly under the resistors was monitored as was the integrity of the resistor interconnects. A 20% increase in the circuit resistance was assumed to be failure. Durability plots were created of vibration cycles to failure versus monitored coupon board strain directly under the resistors The final failure data included results from 26 SnPb soldered LCRs, 39 SAC305 soldered LCRs, 20 SAC105 soldered LCRs and 13 SN100C soldered LCRs. The data included failures that occurred from just under 100,000 cycles to just over 10,000,000 cycles. The data does show that there is very little difference in durability between the SAC305 and SnPb solders. Both solders behaved nearly identically showing nearly the same time to failure at a given load level. Both SN100C and SAC105 solder are not as durable as SAC305 and SnPb under the tested conditions. There was no significant difference in crack paths of the four solders.

Chapter 5: Conclusions, Contributions, and Future Work

5.1 Conclusions

Vibration testing was conducted to generate high cycle fatigue failure data for SnPb and SAC305 solder interconnects. In addition vibration test data for SAC105 and SN100C solder interconnects of resistor parts were provided. The boards were subjected to harmonic vibration testing – BGA boards were subjected to both high and low levels of board excitation, while resistor boards were only subjected to low level board excitation. Strain data of the PWB and resistance data of each component was collected. Time to failure was plotted against board strain range. These tests results were discussed in Chapters 3 and 4 and the conclusions are reviewed here.

5.1.1 BGA Conclusions

The PWB strain ranges versus cycles to failure of each ball grid array component was plotted in log-log space. The clouds of data representing SnPb failures and SAC305 failures showed no significant durability difference between the two solders. A power law regression analysis was conducted on the two data sets and confirmed that there was no significant difference between them. Failure analysis showed that the crack propagation was similar for both solders – cracks appeared on the component side of the solder ball.

5.1.2 LCR Conclusions

The PWB strain range versus cycles to failure of each leadless chip resistor component was also plotted on a durability plot. The failure data shows that there is very little durability difference between the SAC305 and SnPb solders under vibration cycling with failures occurring between 100,000 and 100,000,000 cycles. Both SN100C and SAC105 solder are not as durable as SnPb and SAC305 under vibration cycling. These conclusions were observed in both resistors attached to narrow width pad and resistors attached to standard width pad.

5.2 Additions of Vibration Durability Data to Master Durability Plot

In Patrice Gregory's dissertation [23], LCRs, BGAs and other components were subjected to four point bend tests. The test coupon board construction was exactly the same in material and thickness as the coupons constructed for the tests described in Chapters 3 and 4 (1.6 mm thick Polyclad 370HR). These components were attached to PWBs with SAC305 and SnPb solders. In this section, the vibration high cycle fatigue results discussed in the previous chapters are compared to the four point bending results provided by Ms. Gregory.

Figure 16 shows a durability plot with Gregory's durability data from the four point bend testing, along with BGA durability data from the vibration high cycle fatigue testing [23]. The circle data points represent the SAC305 BGA vibration high cycle

fatigue data, and the red triangles represent the SnPb BGA vibration high cycle fatigue data. This vibration fatigue data was discussed in Chapter 3.

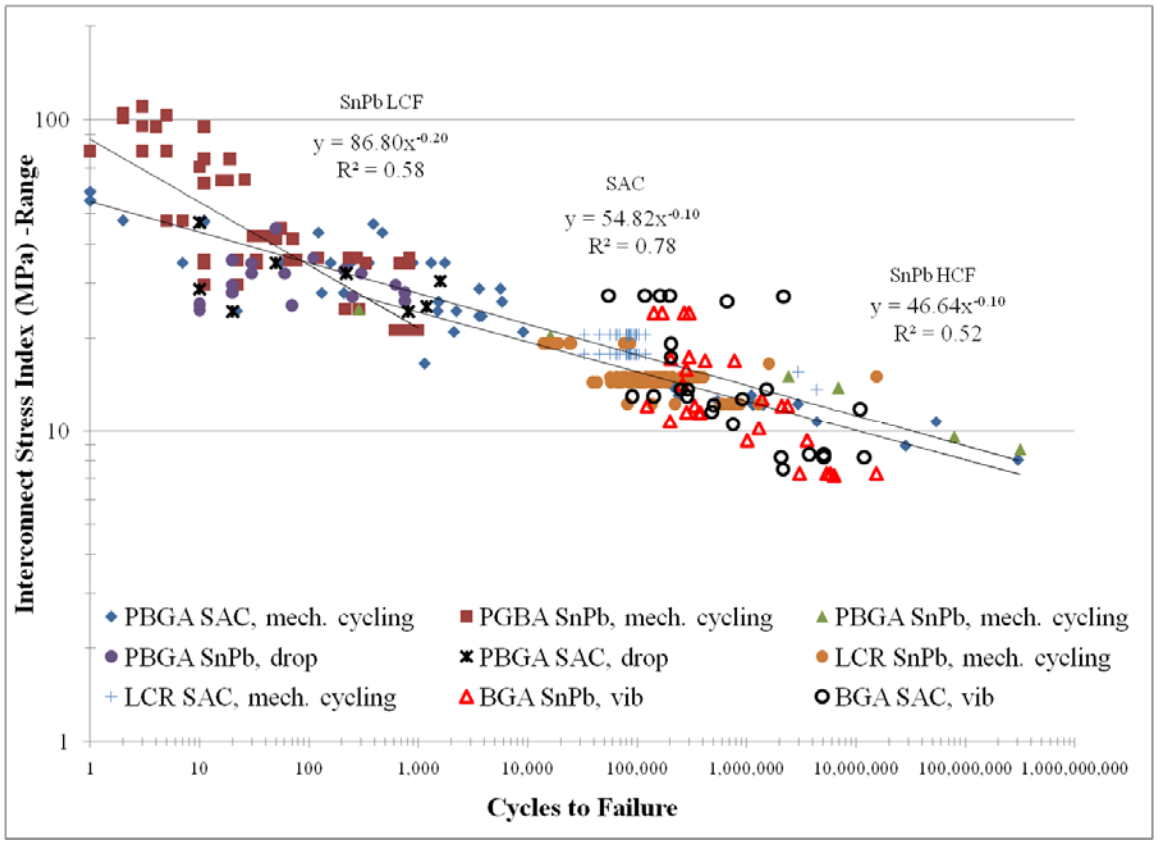

* Mean stress = stress amplitude = ½ range

Figure 16. Durability plot of Gregory's Four point Bend Tests and Vibration BGA tests - Adjusted [23]

Note, the BGA's data from Chapter 3 was adjusted for different BGA sizes, strain measurements and loading conditions than was done in Gregory's testing. The BGA's data in Chapter 3 needed to be adjusted due to the differences in the geometry and array layout of the BGAs used compared to those used by Gregory. The data also needed to be adjusted for the stiffness of the BGA components influencing the PWB strain recorded in the vibration testing since the strain in these tests was measured directly underneath the BGAs, while in Gregory's tests the strain was measured remote from the BGAs. These

adjustments are based on the interconnect stress index range. The stress index range is a calculated 10% volume averaged stress, which was calculated using finite element analysis models from Gregory's dissertation [23], where it is discussed that this index removes any artificial stress concentrations in the computer-generated model yet still identifies the critical stress regions. As described in Gregory's dissertation, a volume average is calculated over 10% of the solder joint in the critical stressed region where a fatigue crack is expected to initiate in the two-dimensional FEA model of the solder joint [23]. This approach is used for thermo-mechanical fatigue and examples can be seen from several other works such as Osterman [26], Darveaux [27][28], Qi[29], and Zhou[30].

Gregory conducted testing that ranged from some maximum board strain to zero board strain. The vibration testing in Chapters 3 and 4 was fully reversed loading. The adjustment in the abscissa, PWB strain range, can be done using the Goodman diagram [24]. This calculation is shown in Appendix F.

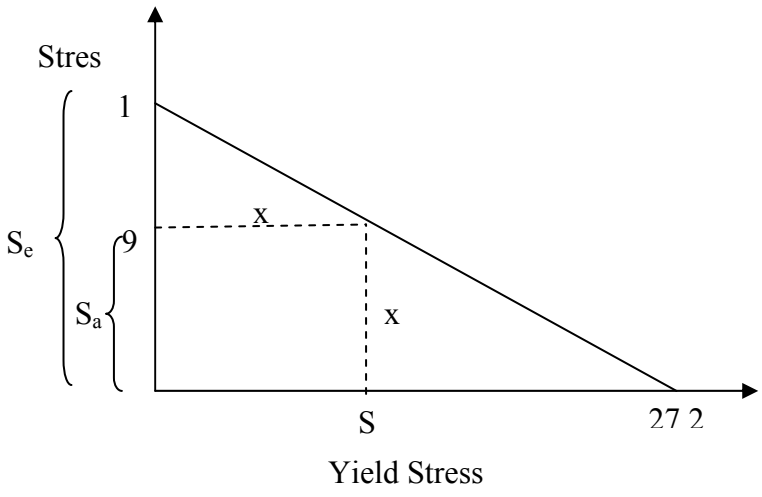

Figure 17. Modified Goodman diagram with calculated correction factors for fully reversed loading [23]

Figure 17 shows the modified Goodman diagram with the calculated ratios for the BGAs subjected to the fully reversed loading in the vibration high cycle fatigue versus the BGAs subjected to tension-tension loading in the four point bending [23]. This diagram is used to determine appropriate conversion factors for different loading condition scenarios [24]. In Gregory's dissertation, the ratio to use was calculated and the vibration high cycle PWB strain range was adjusted. The amount to reduce the stress in the BGAs subjected to the fully-reversed loading was calculated in Gregory's dissertation, and was found to be 9/11 [23]. Figure 16 shows the adjusted durability plot with the abscissa being the interconnect stress index. With the adjustment, note that the BGAs subjected to the vibration high cycle fatigue are in agreement with the data from Gregory's earlier four point bend tests.

When the BGA data was discussed in Chapter 3, a power law regression fit was made to the failure data. The regression fit was nearly identical between the SAC305 and SnPb solder, demonstrating that the durability between the two solders was basically the same. The fatigue exponent, as determined from the regression analysis, was about 4.5 from failure data between 100,000 and 10,000,000 cycles. In the discussion in Chapter 3, it was indicated that this value seem reasonable for an accelerated test. When the Chapter 3 vibration data is viewed in context of more failure data as seen in Figure 16, one should question the previous regression analysis. It is dangerous to try and determine fatigue exponents from test data over a limited range, two orders of magnitude, when the failure scatter for a set PWB strain range is within one order of magnitude. One needs to be

careful with the uncertainty in the regression coefficients as well as paying attention to the coefficient of determination (R^2), which in this case was not very good at 0.6.

Gregory's LCR four point bend data is also compared with the vibration test results of Chapter 4. Only the SAC305 and SnPb data is compared. Figure 19 shows the durability plot of PWB strain range versus number of cycles to failure of the 2512 leadless chip resistors. The strain for the LCR vibration data was adjusted in similar fashion to the BGA vibration data since the strain was measured directly underneath the resistors. In the plot, Gregory's resistors are identified with solder type and "mech cycling" while the resistors from Chapter 4 are labeled with solder type and "vibration". Only the standard pad resistors from Chapter 4 are used because these pads were the same as Gregory used. It is not possible to include the narrow pad resistor data without a detailed finite element analysis to compute a stress index. This complex, three-dimensional finite element analysis is beyond the scope of this thesis.

An approximation can be attempted to include the narrow pad resistor durability data to the standard pad resistor durability data. The size of the narrow pad is one fifth the size of the standard pad. Assuming the stress-strain relationship for these solders is linear, one can estimate that the stress experienced by the narrow pads are five times that of the standard pad. Making this adjustment, this puts the narrow pad data above the other data sets as shown in the durability plot in Figure 18. The yellow squares represent the SnPb narrow pad approximations while the SAC305 narrow pad approximations are represented by the pink triangles. As discussed in Chapter 4, this shows that a simple approximation is not appropriate for this data set since there is still a wide spread in the data. Therefore, it is recommended in the future to conduct finite element analysis on the

narrow pad resistors to determine its stress index that can better compare the two different size pads.

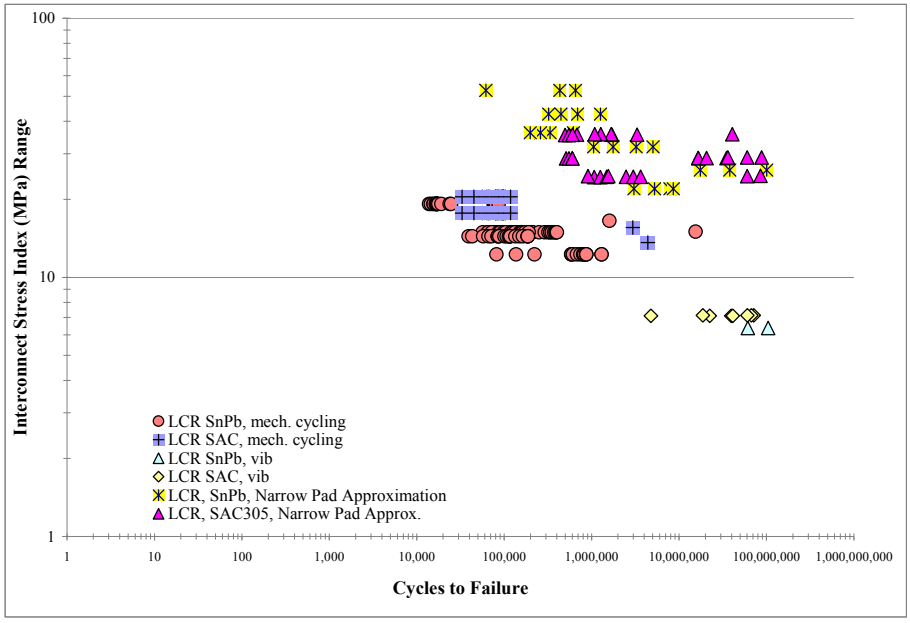

Figure 18. Durability plot of 2512 LCR data with unadjusted narrow pad LCR failure data

The test coupons for both Gregory and Chapter 4 were the same thickness and nearly the same construction, thus PWB strain is used as the abscissa in the durability plot shown in Figure 17. The PWB strain range for the vibration test results was adjusted as described earlier to account for the different loading (tension-compression versus tension-tension). PWB strain rates for the vibration data were on the order of 3×10^{-1} per second while Gregory's mechanical cycling PWB strain rates were an order of magnitude lower. The yellow diamonds represent the SAC305 vibration failures, and the SnPb vibration failures are represented by the light blue triangles. The circles represent failures of SnPb four point bend failures and the squares represent the SAC305 four point bend failures. It must be pointed out that the vibration failure data is only the first failures from a group of resistors and not a data set of complete failures. Due to testing limitations

the standard pad resistors on the vibration test coupon rarely failed. The vibration tests were terminated before all the resistors in a column failed. This is in contrast to the data in the bend testing, where testing continued until almost all of the resistors had failed. Regardless, the plot shows that the vibration failure data are at lower PWB strain ranges, but the cycles to failure are significantly higher than the four point bend test failures. Looking at only this plot, it may appear that the mechanical cycling durability and the vibration durability results differ, but when viewed in context of more data this conclusion does not hold.

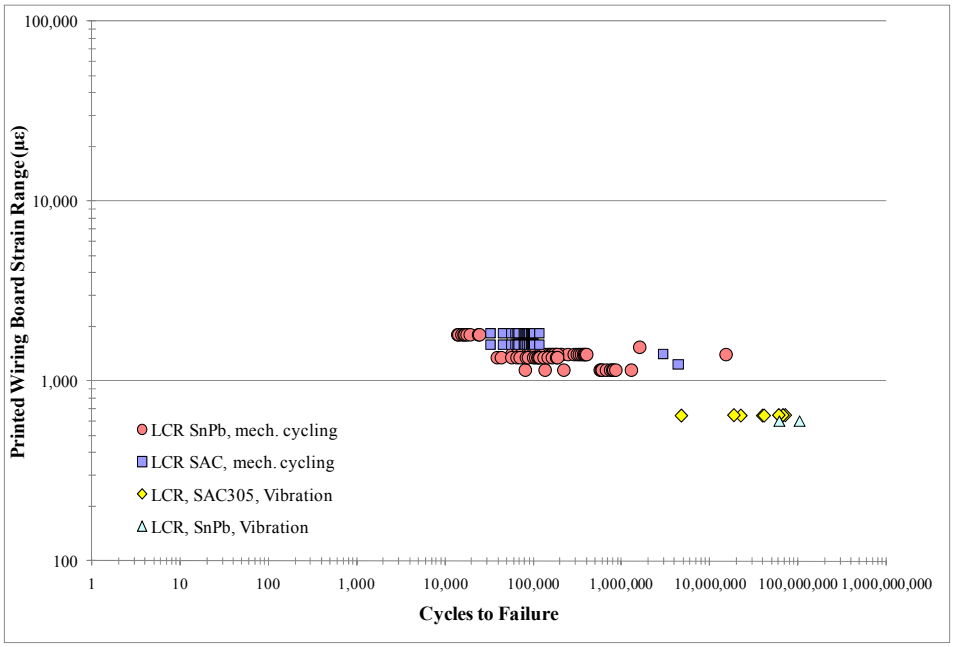

Figure 19. Durability plot of Gregory's four point bend LCR test data and vibration LCR standard pad test data [23]

Figure 20 shows a compilation of all the SnPb failures from Gregory and the testing conducted in this thesis with BGAs and the LCR standard pads for only SnPb failures. Figure 21 shows the same data for only the SAC305. In these plots, the abscissa

is the interconnect stress index rather than PWB strain range because of the different component families and geometries. (As discussed earlier,the interconnect stress index is a calculated 10% volume averaged stress, which was calculated using finite element analysis models from Gregory's dissertation [23]). Figure 21 combines the data from Figure 4 and 5 into a single plot for both solder types.

When the vibration results for the SnPb standard pad resistors, only 2 data points, are viewed in Figure 19, it appears as if the vibration durability is worse than Gregory's 4-point bending LCR failures. But when viewed in context of a larger data set as seen in Figure 20, the vibration failures (the "+" data points) do not deviate significantly from the rest of the failure data. They are a little low, but not out of line.

Similarly when the vibration results for SAC305 standard pad resistors, eight data points in Figure 19, the failures appear to indicate a lower durability that Gregory's LCR SAC305 data. When viewed in context of a larger data set as seen in Figure 21, the vibration failures (the "X" data points) do not deviate significantly from the rest of the failure data.

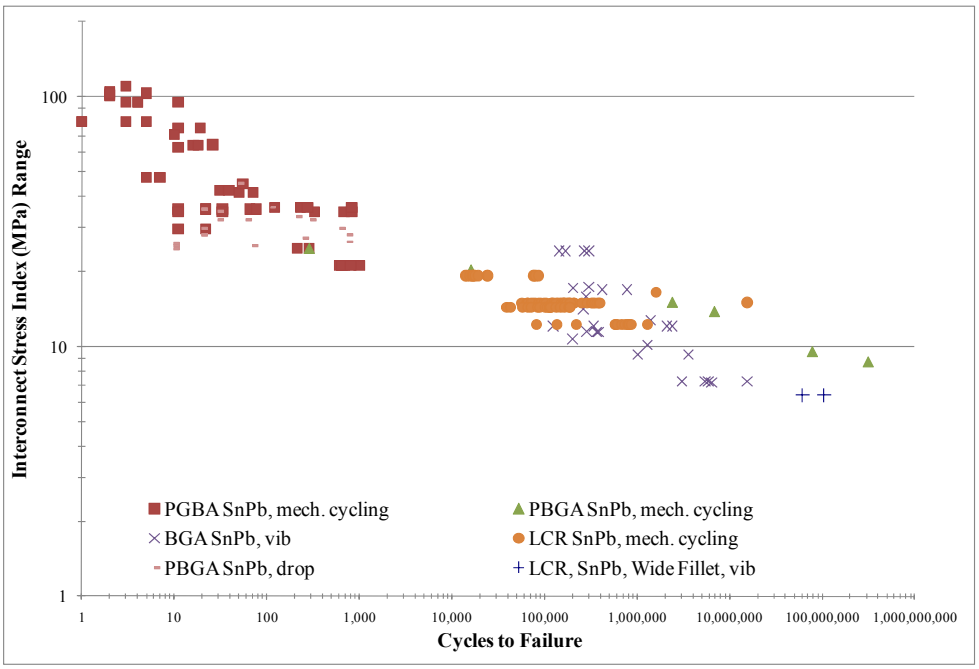

Note: plot is for condition where mean stress = stress amplitude = ½ range

Figure 20. Durability plot of all of Gregory's test data, Chapter 3 vibration BGA data, and Chapter 4 LCR standard pad test data for SnPb[23]

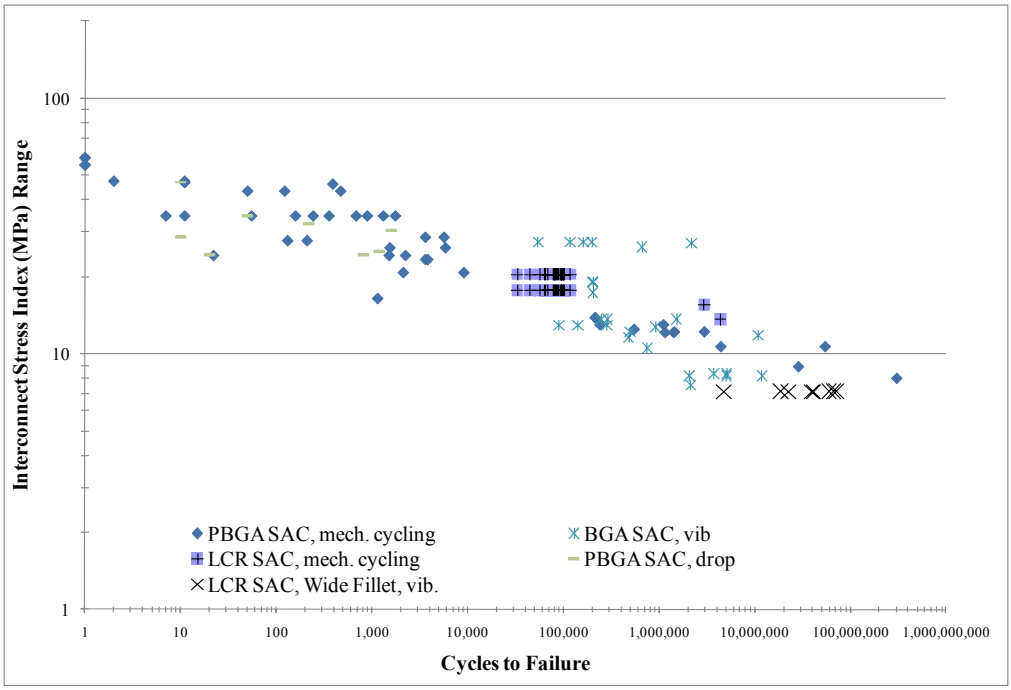

Note: plot is for condition where mean stress = stress amplitude = ½ range

Figure 21. Durability plot of all of Gregory's test data, vibration BGA data, and LCR standard pad test data for SAC305 [23]

Figure 22 combines the data from Figure 20 & Figure 21. It is recommended that this lower bound of data can be used as criteria for designing electronic components attached to PWBs with these solders. It is also concluded that it is dangerous to look at durability plot over a finite range of cycles to failure. It was noted in Chapter 3 that the regressions conducted with a data set that only had a limited range of cycles to failure is very different from the overall regression of all of the solder data as seen in Figure 20-Figure 22.

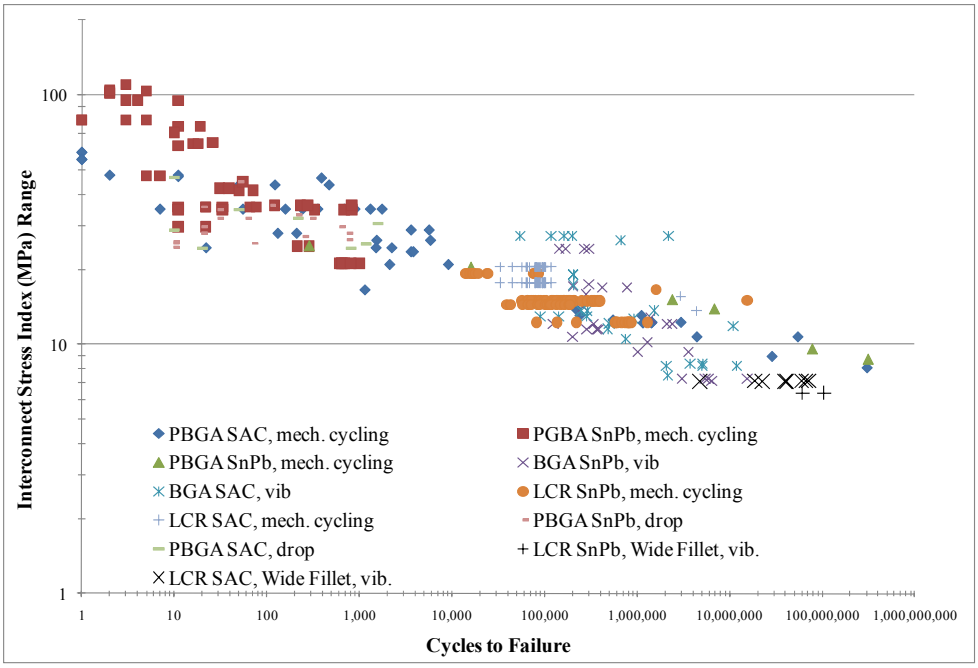

Note: plot is for condition where mean stress = stress amplitude = ½ range

Figure 22. Durability plot of all of Gregory's test data, vibration BGA data, and LCR standard pad test data for both SnPb and SAC305 [23]

Figure 23 is Figure 22 re-plotted to more clearly identify the SnPb solder failures (purple squares) and the SAC305 solder failures (black diamonds). This was purposely done to show the data sets, or data clouds, of the two solder types are very similar. This

indicates that the durability of the two solders in the tested ranges may be considered the same. A power law regression was conducted on the two data sets and the results are also shown in the figure.

Theoretically one should not conduct a single power law regression from very low cycles to failure through a very large number of cycles to failure due to the change in the basic fatigue mechanism from low cycle fatigue, driven by plastic strains, to high cycle fatigue driven by elastic strains. Traditionally one should see a distinct low cycle fatigue region and a high cycle fatigue region, each having a unique power law fit. Gregory noted that this distinct transition between low cycle fatigue and high cycle fatigue is not seen due to a shift in failure mechanisms. For very low cycles to failure, the dominant failure is copper traces and land pull-outs. For high cycles to failure, the dominant failure is classical solder fatigue cracks. However, if one is just interested in the integrity of the solder interconnect, and not exactly what has failed, then a single power law regression over the entire range seems to work.

As shown in Figure 22, the regression lines for SAC305 and SnPb are very close to each other. The fatigue exponent for SAC305, inverse of the power law exponent, is a little over 9 while the fatigue exponent for SnPb is about 8. Theoretically this exponent indicates that the SAC305 solder is a little more durable than the SnPb for high cycles. It is also seen where the SAC regression line is above the SnPb regression. But it must be noted, and as pointed out by Gregory, the SnPb solder did show some low cycle fatigue behavior where it clearly outperformed the SAC305 solder under ultra low cycles to failure, less than 10 cycles. These data points are influencing the overall regression fit and making the SnPb regression line steeper than it should be. These data points were

from failures that were from the PWB (copper trace cracking and copper pad pullout) which do not involve the solder attachments as discussed in Gregory's dissertation [23]. These data points are influencing the solder durability curves when the failures are not even caused by the solder. This effect can be seen in the next figure, when the early failures are excluded from the regression. It is necessary to exclude these very early failures because of the failure mode and because of the high influence on the regression.

The durability of the two solders are closer than these two regression lines show. Figure 23 shows all data and regression lines for the data, both SnPb and SAC305 failures, include the cycles to failure of 10 or more cycles. The failures that occurred before 10 cycles are shown in the figure for reference. The white squares represent the SnPb failures that happened under 10 cycles and the white diamonds represent the SAC305 failures that happened under 10 cycles. Note the regression lines are now nearly parallel between the two solders and the SnPb solder is just slightly lower. Looking at the 95% confidence intervals of the SnPb and SAC305 regression coefficients and the regression exponents, they overlap. This can be seen in Table 5 and Table 6. Accounting for this, the durability difference of the two solders is negligible.

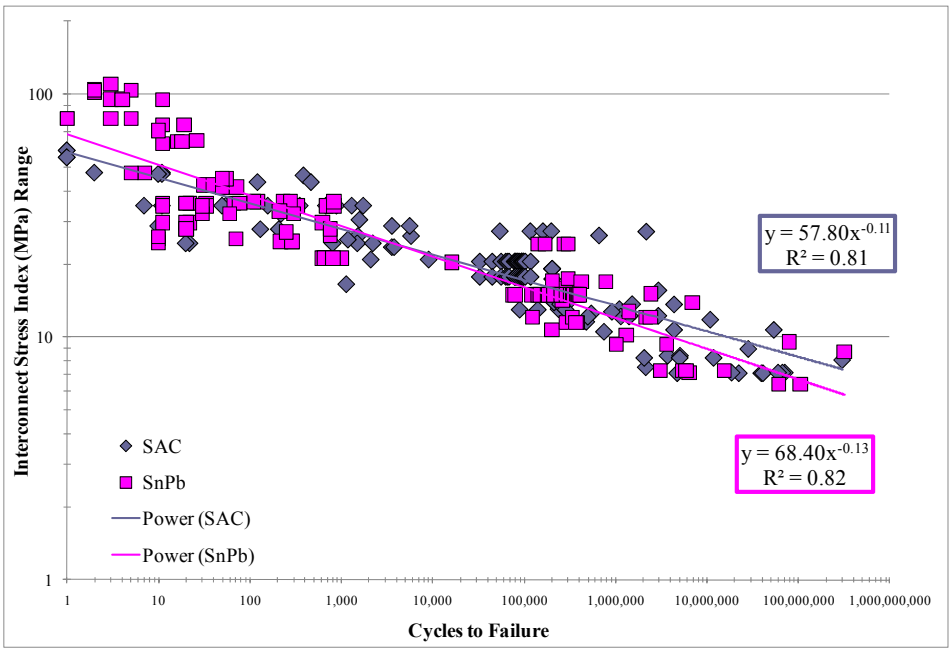

Note: plot is for condition where mean stress = stress amplitude = ½ range

Figure 23. Durability plot of all of Gregory's test data, vibration BGA data, and LCR standard pad test data for both SnPb and SAC305 Combined [23]

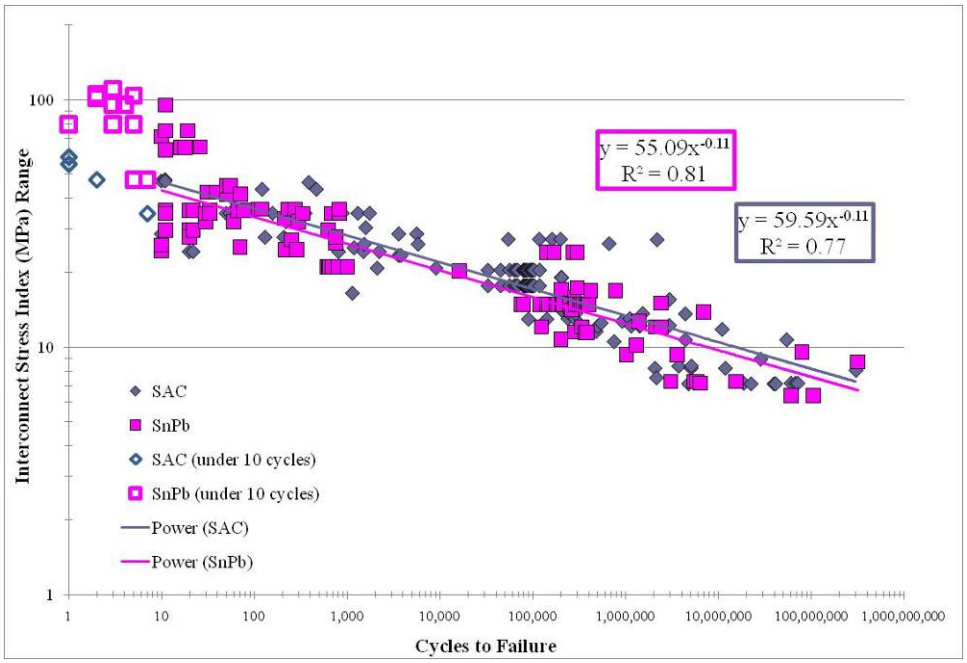

Note: plot is for condition where mean stress = stress amplitude = ½ range

Figure 24. Durability plot of all the data (Figure 7) where the regression analysis excludes any data where the cycles to failure are less than 10 cycles

SnPb Regression Analysis

	Mean	Upper 95%	Lower 95%
Coefficient	55.1	64.9	46.8
Exponent	-0.11	-0.10	-0.12

Table 5. Analysis on master SnPb durability regression

SAC305 Regression Analysis

	Mean	Upper 95%	Lower 95%
Coefficient	59.6	67.1	52.9
Exponent	-0.11	-0.10	-0.12

Table 6. Analysis of master SAC305 durability regression

The area under the data clouds is the "safe area" where a designer can be comfortable using either SAC305 or SnPb solders attaching components to PWBs. The SnPb regression was used to determine a standard deviation. The safe area limit was calculated to be three times the standard deviation below the SnPb regression. There is a 99.7% guarantee that no failures will occur underneath this line. The area under the generated line is deemed a safe area, which can serve as a design goal for BGA and LCR survivablity during circuit board design. Figure 25 shows this failure-free area.

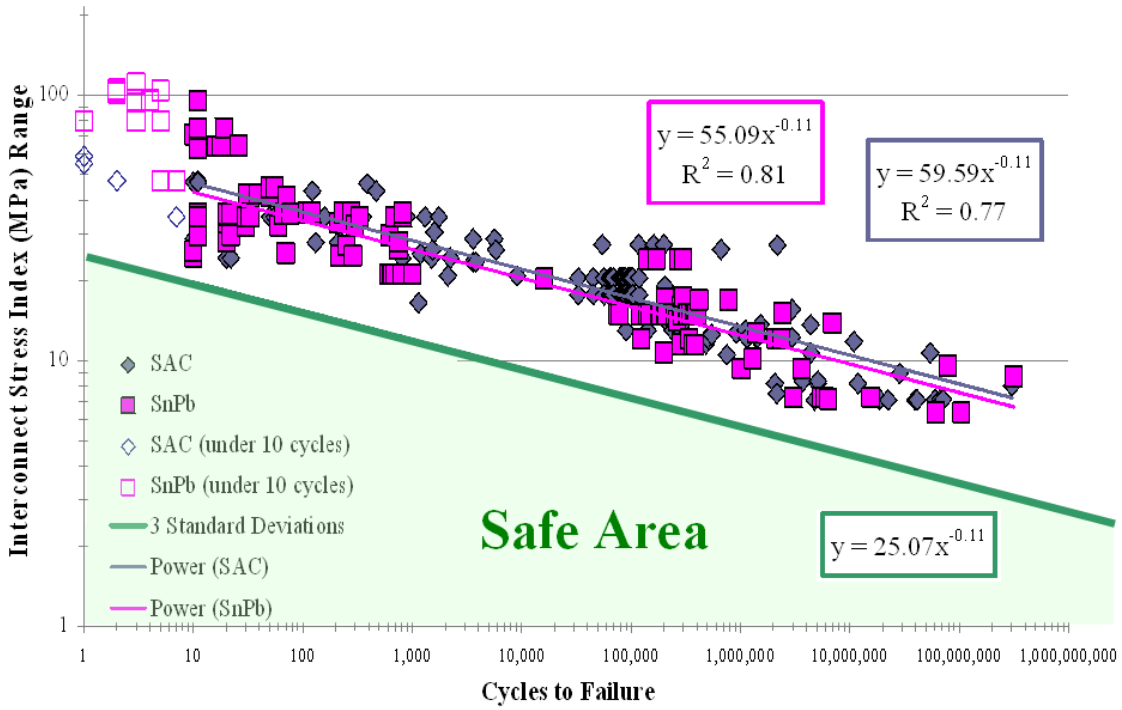

Note: plot is for condition where mean stress = stress amplitude = ½ range

Figure 25. Durability Plot of SAC305 and SnPb with Calculated "Safe" Area for Designers

5.3 Contributions

There is not much literature currently available on the topic of high cycle fatigue life for lead-free solders. This work will make data on high cycle fatigue of lead-free solders available. The failure data has shown that the SnPb and SAC305 solder attachments are very similar in durability. This was again proven on a newly-generated master durability plot with previously-generated failure data from Gregory's analysis [23]. The master curve contains the data generated from the high cycle fatigue tests described in this thesis. Adding the high cycle fatigue data again confirms that the SAC305 and SnPb solders are very similar in durability, which was also shown by Gregory [23]. This new master durability plot provides guidance to those who need to replace standard SnPb solder with Pb-free solder in their products. A safe area was

determined in Figure 25 which can be used by designers of electronic products who have to design products using SnPb and SAC305 solder attachments that have to withstand high cycle fatigue. This shaded area in the figure can be used as a design goal for survivablity during circuit board design. The line can be adjusted using the desired number of standard errors to serve as an additional saftey factor. The SN100C and SAC105 data from the resistor testing also confirms that these solders are less durable than the SAC305 and SnPb solders. This should also aide designers when having to choose between the SAC305, SAC105 and SN100C.

5.4 Future Work

The following sections suggest changes to the test coupon designs and additional work that could prove useful for durability comparisons.

5.3.1 Future Work for BGAs

The board design of the BGA test coupons can be improved. The outer four BGAs rarely failed because the board experiences a very small amount of flexure or even no flexure at the location of these outer BGAs. It is recommended that these BGAs on the outside be removed. More testing on BGAs can be done to generate more durability data on a larger range of cycles to failure if desired.

5.3.2 Future Work for Leadless Chip Resistors

The scatter in the Weibull plots of the leadless chip resistors was concluded to be due to defect-driven failures. The outermost columns of resistors

never failed due to the fact these locations of these outer columns happened to be in the nodes of the board where no flexure occurs. It is recommended that the resistor board design be revised, removing these outermost columns of resistors.

An FEA model of the narrow pad resistors is to be constructed to provide a more accurate approximation to better compare the narrow pad resistor durability data to the other components' durability data. Once that is accomplished, the narrow pad durability data can be added to the master durability plot. More resistor boards with the ENIG finish will need to be tested at the same strain levels, and this data can be added to the existing Weibull plots – this will make the Weibull plots a better tool with more data points. Additionally, boards with different finishes, for instance, OSP, finish can be tested and compared to the durability data from boards with the ENIG finish.

5.3.3 Future Work for Testing Environment

The testing environment was not controlled. Temperatures changed with the outside temperatures, which ranged from approximately 10 °C to 32 °C. Further testing should be done with temperature as an additional variable. It would be interesting to see if this similarity in durability is the same near freezing conditions and at much hotter temperatures.

Appendix

A. Index

B. *Weibull Plots of BGAs*

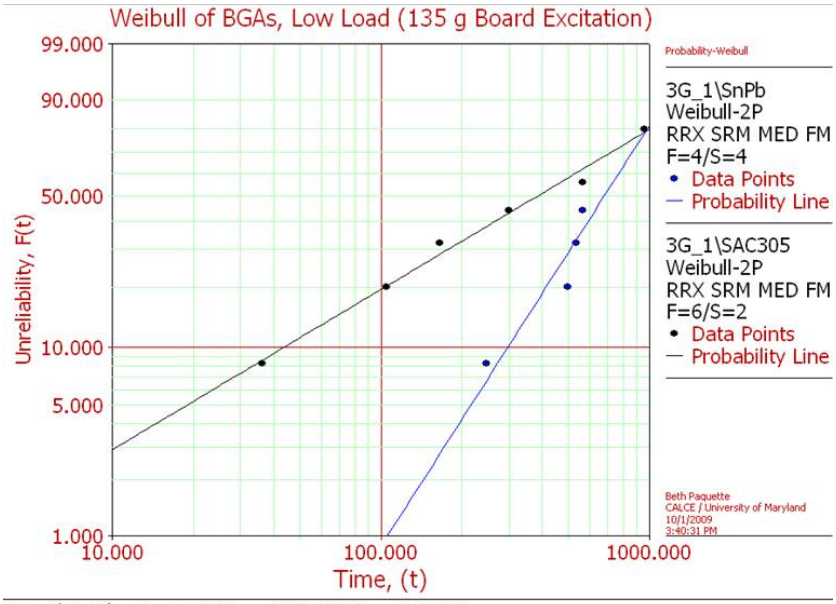

Figure 26. Weibull plot of SnPb and SAC305 BGAs at 135 g board excitation

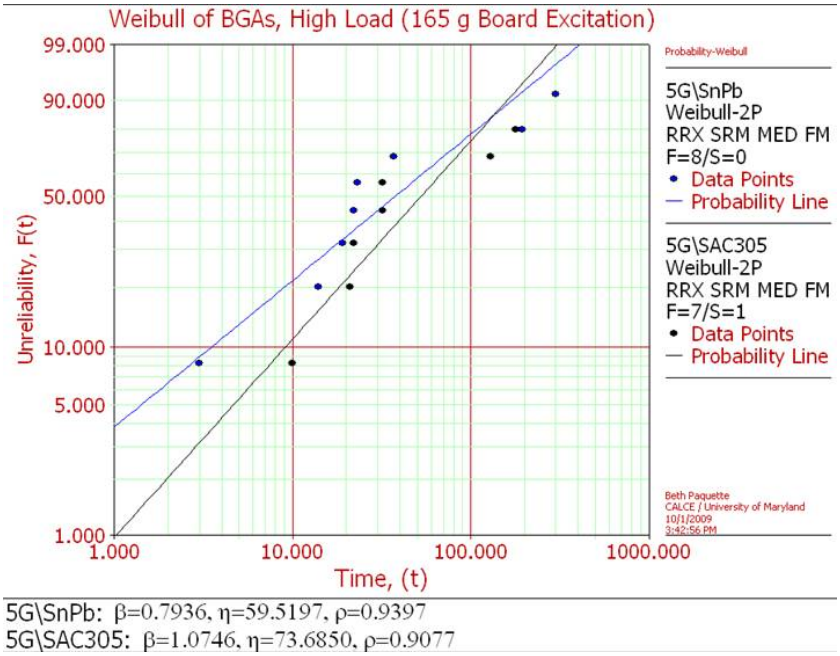

Figure 27. Weibull plot of SnPb and SAC305 BGAs at 165 g board excitation

C. *BGA Cross Sections*

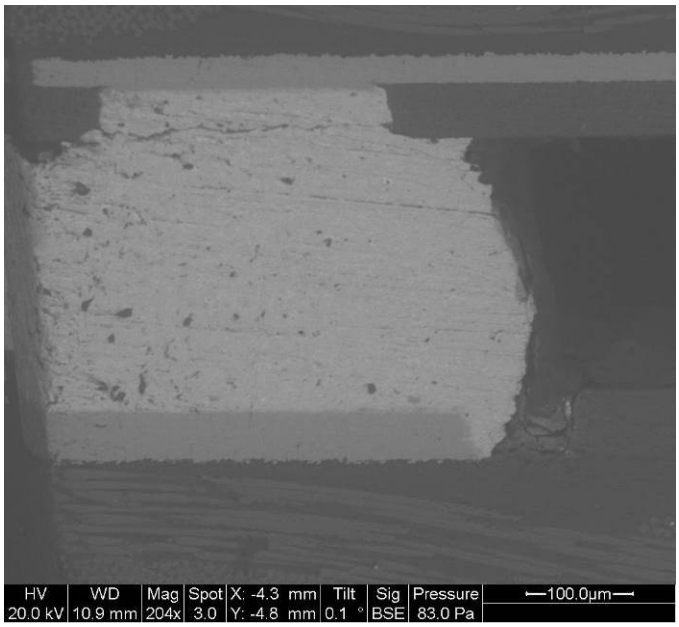

Figure 28. Cross section of corner SnPb solder ball, component U4, ball A14
BGA cross-section cornered

Figure 29. Cross section of corner SnPb solder ball, component U4, ball P1
BGA cross-section cornered

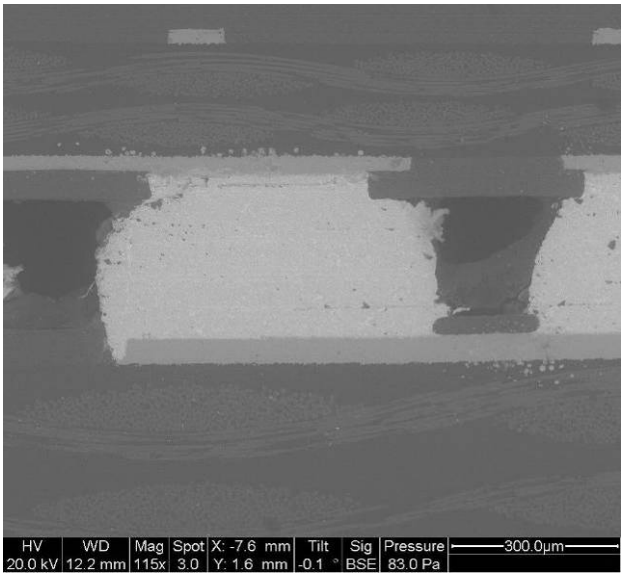

Figure 30. Cross section of corner SnPb solder ball, component U4, ball P2

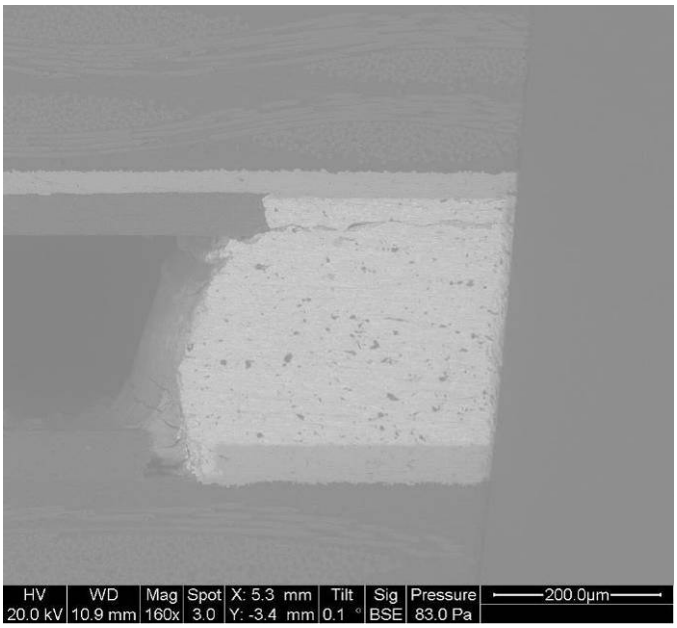

Figure 31. Cross section of corner SnPb solder ball, component U4, ball A1
BGA cross-section cornered

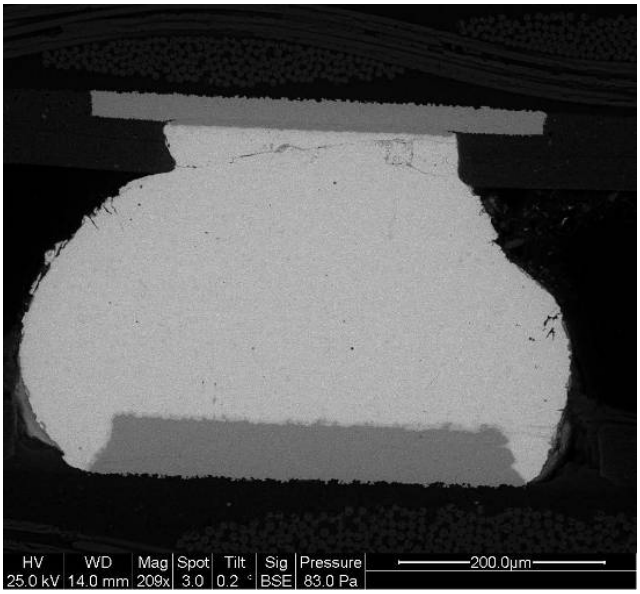

Figure 32. Cross section of corner SAC305 solder ball, component U6, ball A1

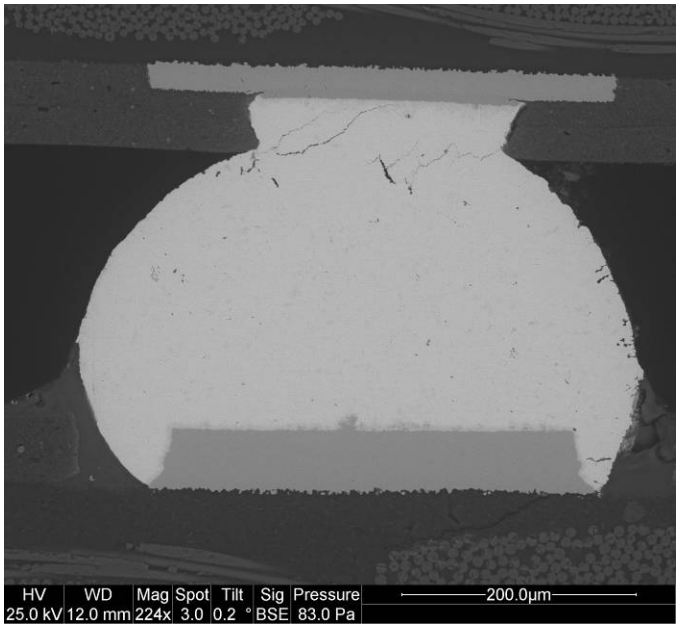

Figure 33. Cross section of corner SAC305 solder ball, component U6, ball P14

D. *LCR Weibull Plots*

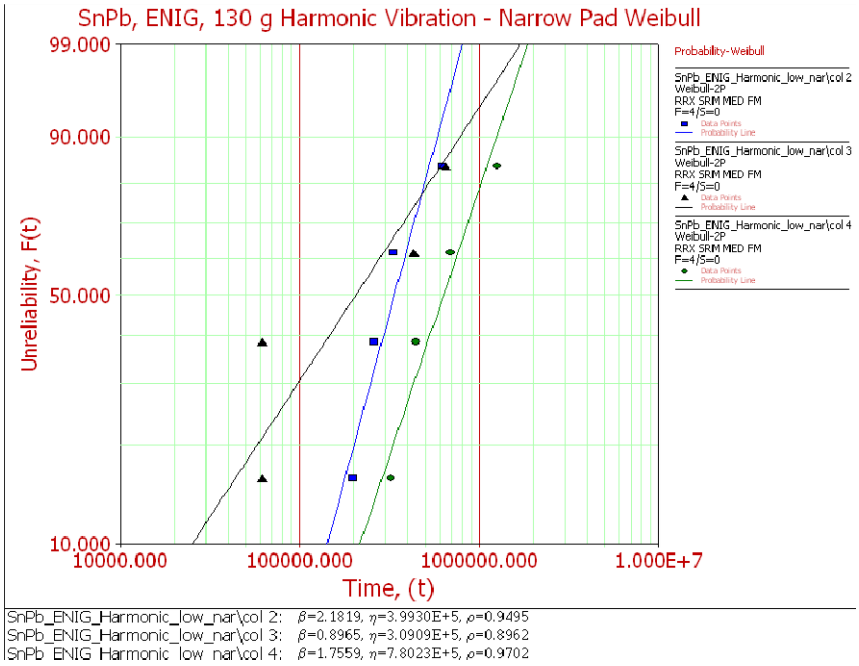

Figure 34. Weibull plot of SnPb narrow pad failures, 130g board excitation

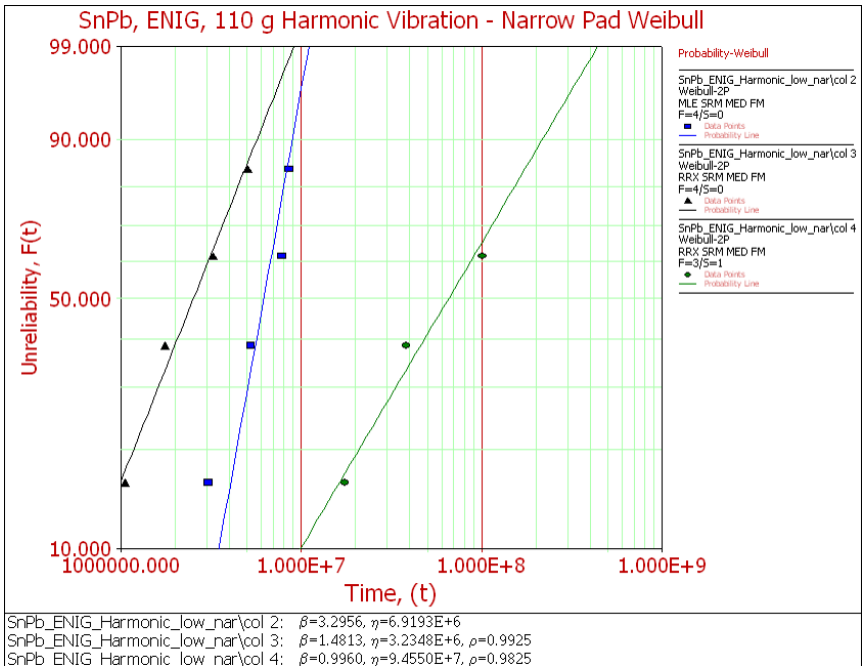

Figure 35. Weibull plot of SnPb narrow pad, 110 g board excitation

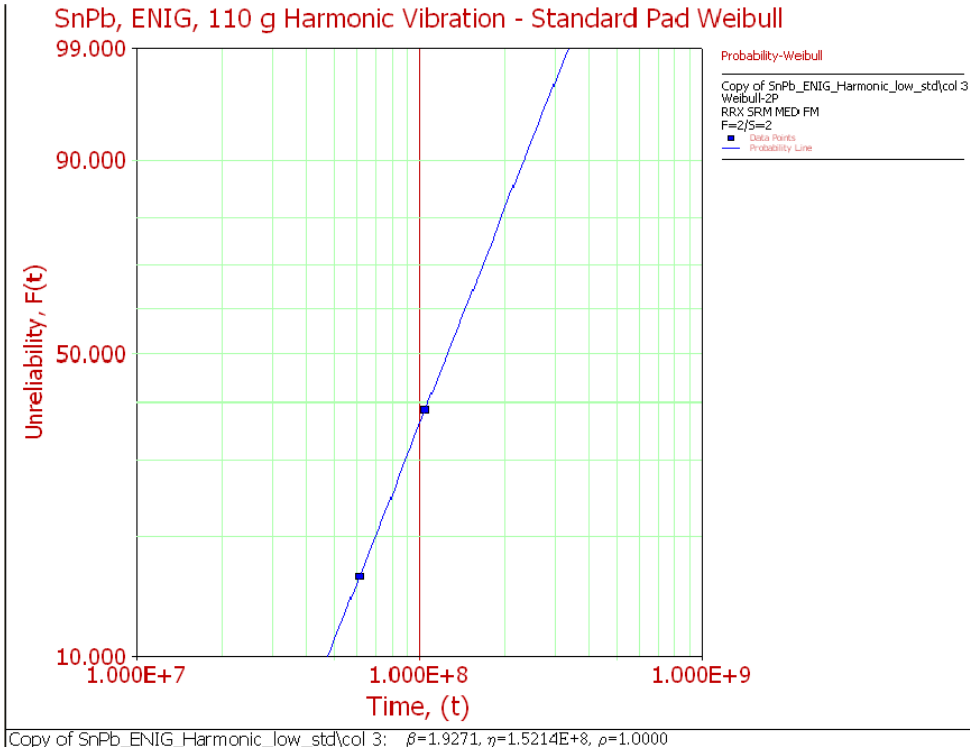

Figure 36. Weibull Plot of SnPb Standard Pad, 110 g board excitation

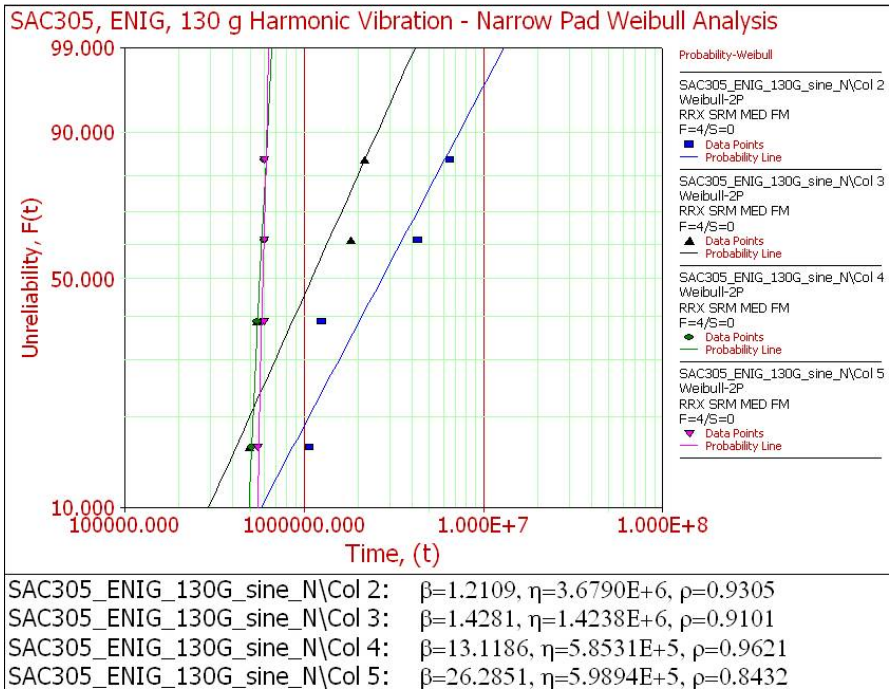

Figure 37. Weibull Plot of SAC305 narrow pads at 130 g board excitation

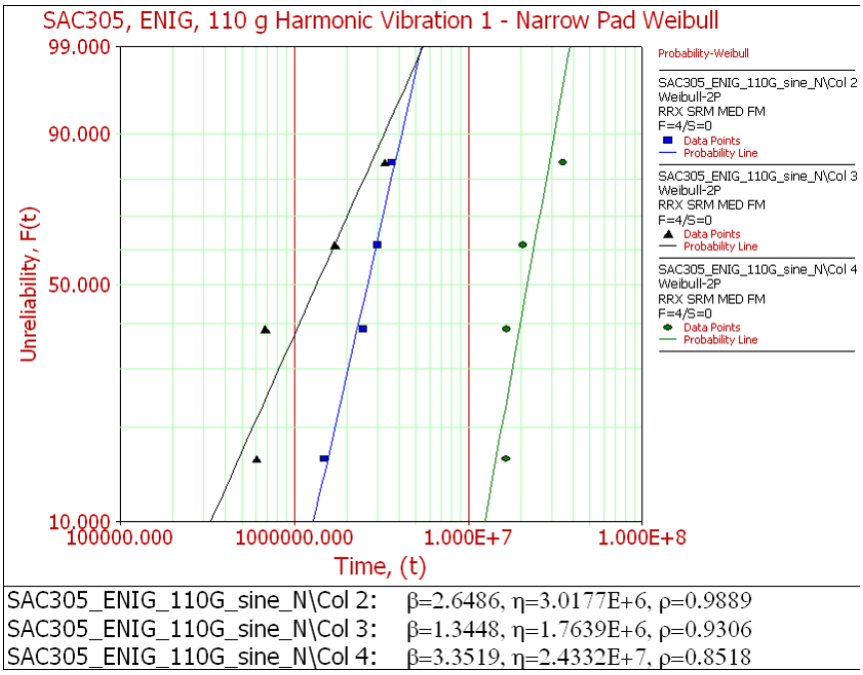

Figure 38. Weibull plot of SAC305 narrow pad, test 1, 110 g board excitation

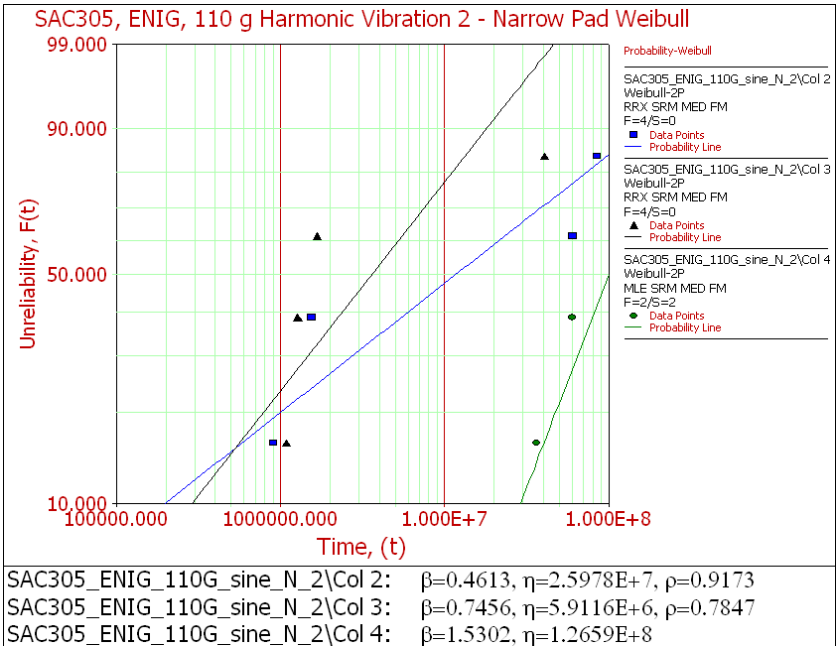

Figure 39. Weibull plot of SAC305 narrow pad, test 2, 110 g board excitation

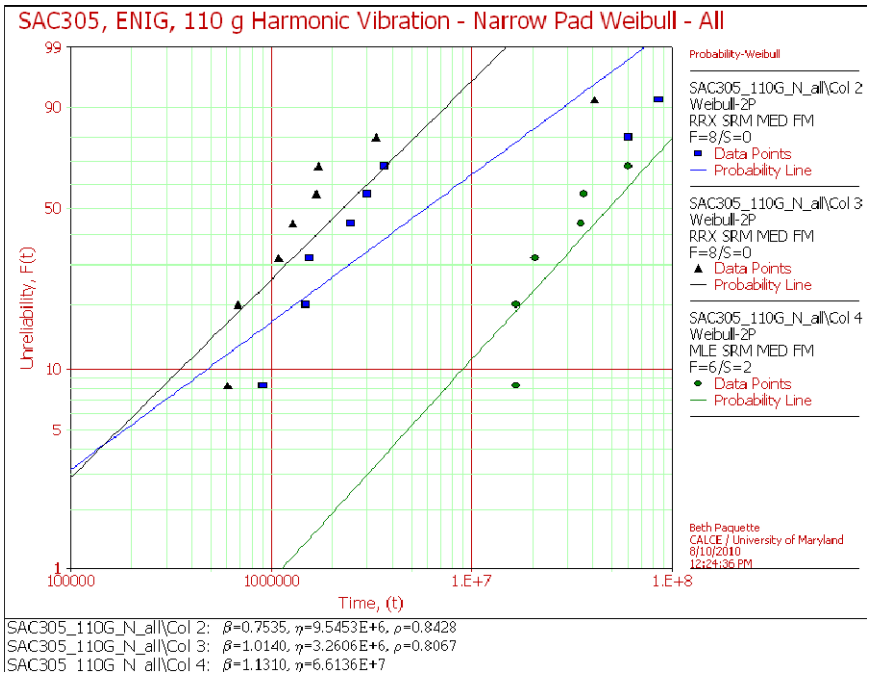

Figure 40. Weibull plot of SAC305 narrow pad, tests 1 and 2 combined, 110 g board excitation

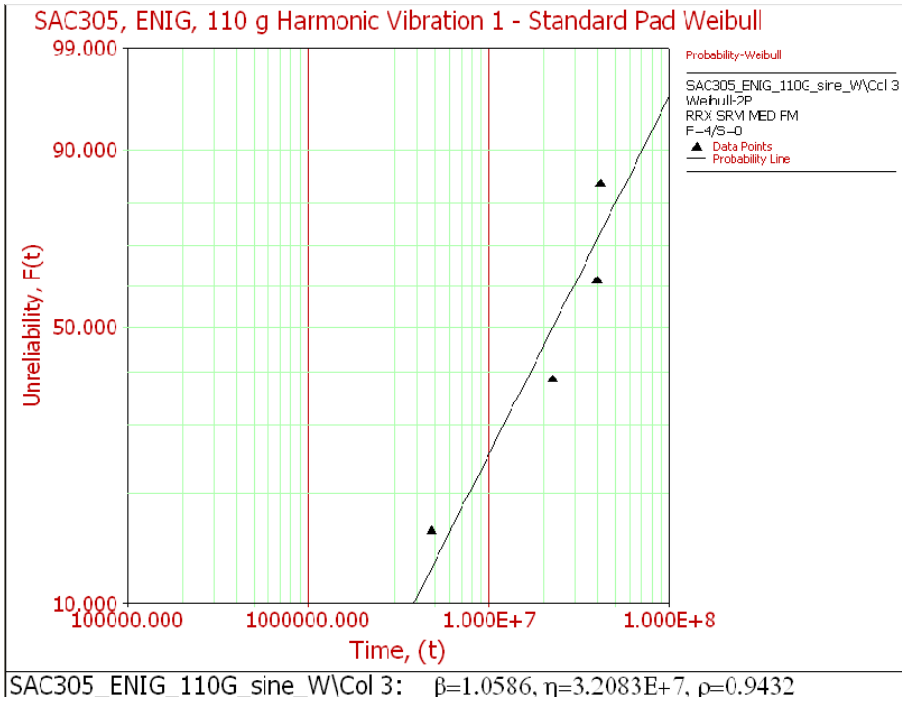

Figure 41. Weibull plot of SAC305 standard pad, Test 1, 110 g board excitation

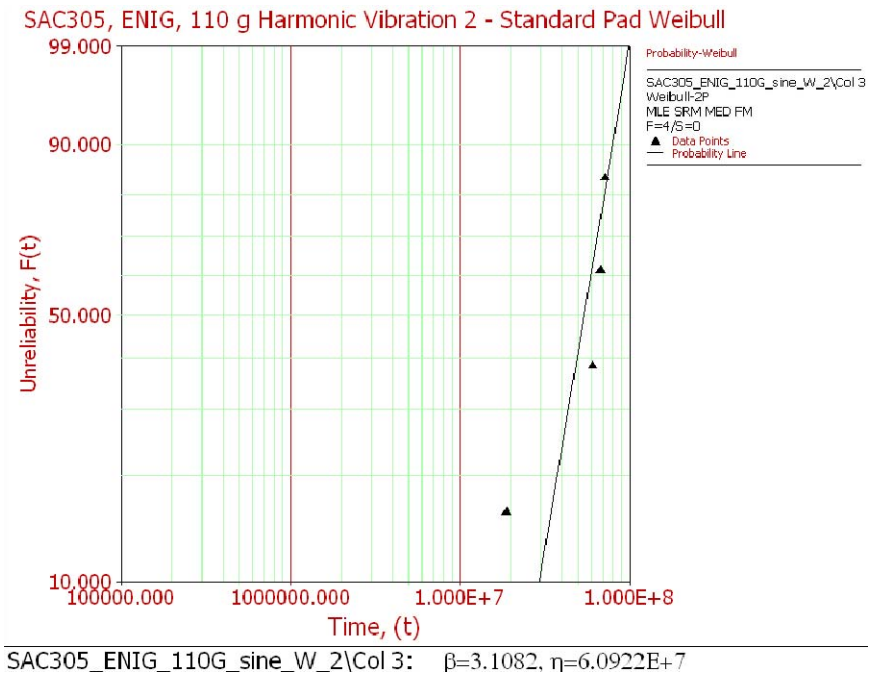

Figure 42. Weibull plot of SAC305 standard pad, test 2, 110 g board excitation

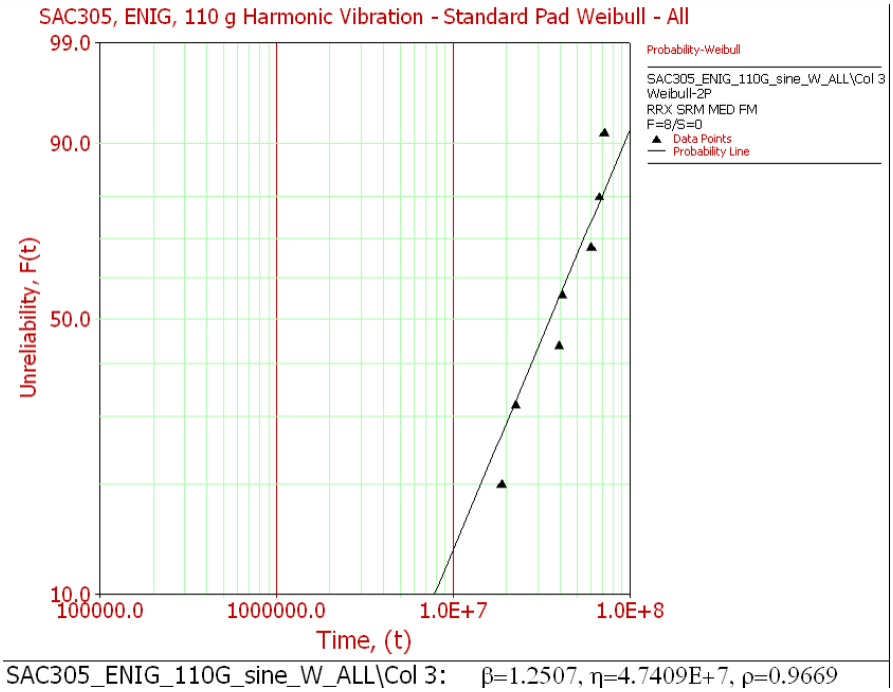

Figure 43. Weibull plot of SAC305 standard pad, tests 1 and 2 combined, 110 g board excitation

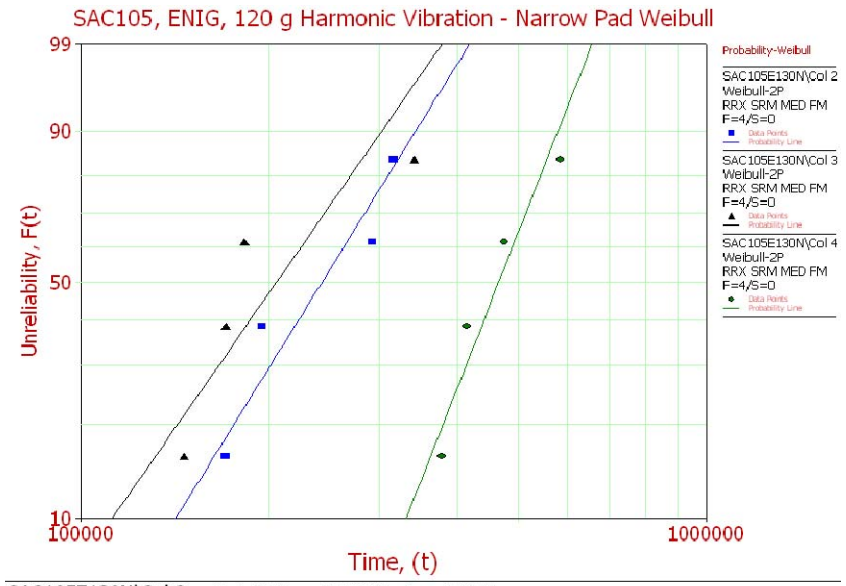

SAC105E130N\Col 2: β=3.4966, η=2.7000E+5, ρ=0.9531
SAC105E130N\Col 3: β=3.1130, η=2.3145E+5, ρ=0.8690
SAC105E130N\Col 4: β=5.5291, η=4.9770E+5, ρ=0.9595

Figure 44. Weibull plot of SAC105 narrow pad, 120 g board excitation

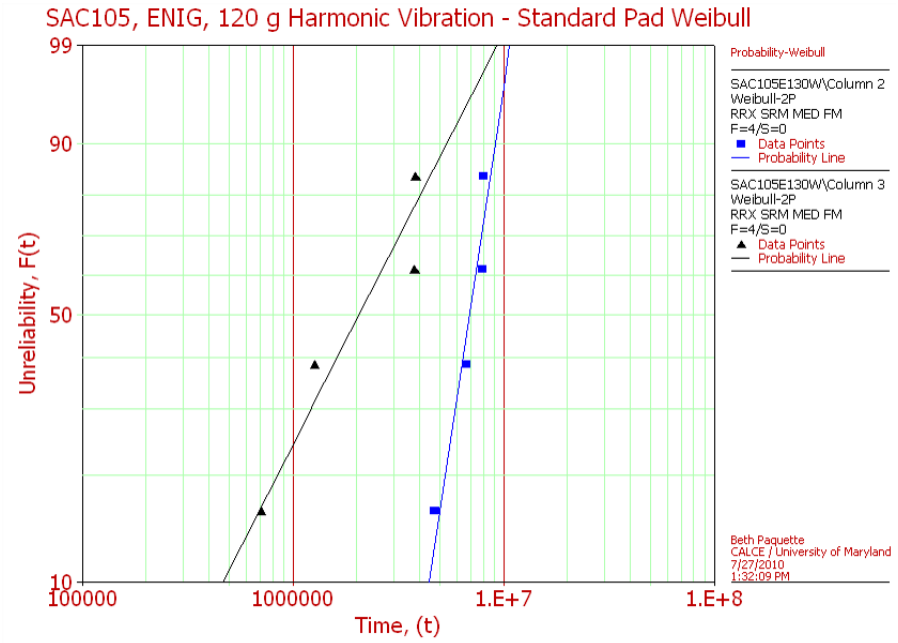

SAC105E130W\Column 2: β=4.2848, η=7.4945E+6, ρ=0.9563
SAC105E130W\Column 3: β=1.2628, η=2.7680E+6, ρ=0.9531

Figure 45. Weibull plot of SAC105 standard pad, 110 g board excitation

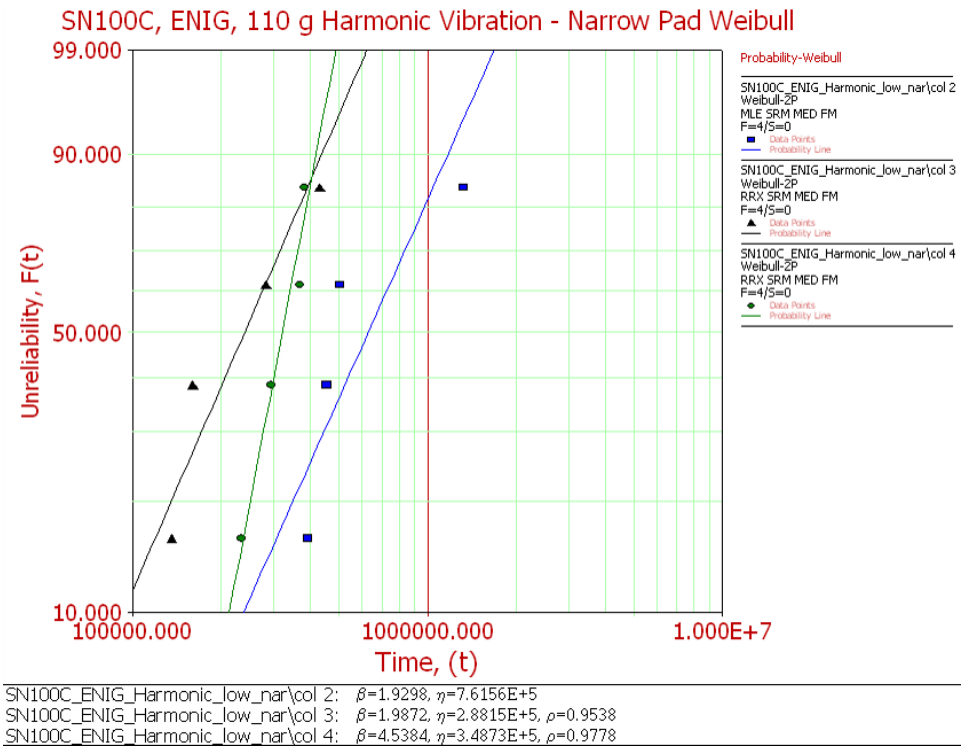

Figure 46. Weibull plot of SN100C narrow pad, 110 g board excitation

E. Leadless Chip Resistor Solder Cross Sections

Note: All boards were ENIG finish as stated in Chapter 4.

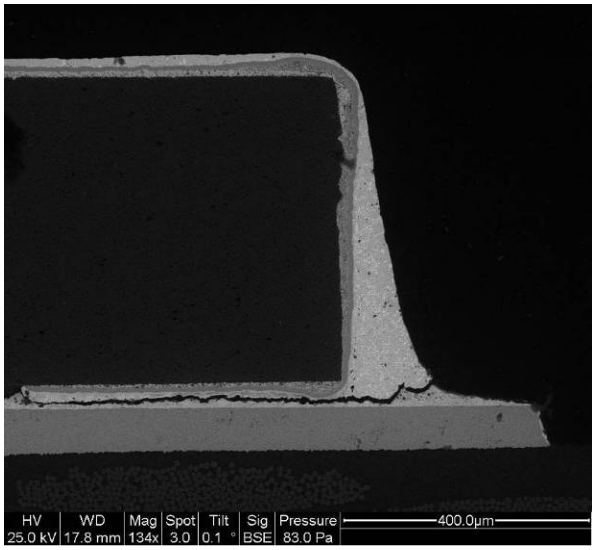

Figure 47. Solder crack of SnPb, resistor 3 (narrow pad), failed at 432,600 cycles

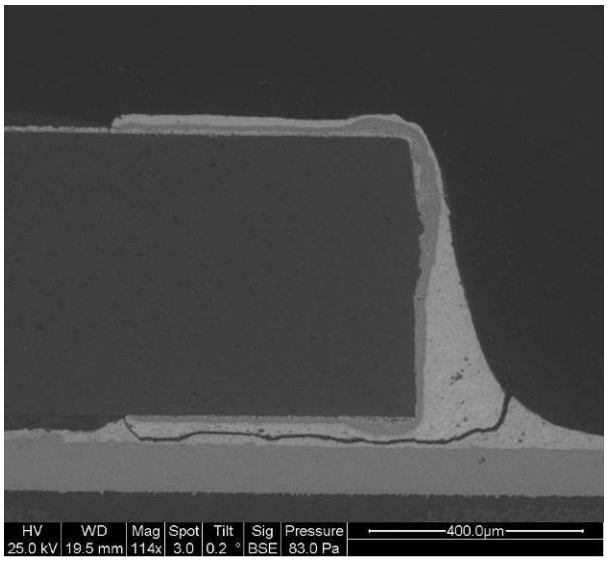

Figure 48. Solder crack of SnPb, resistor 29 (narrow pad), failed at 38,093,100 cycles

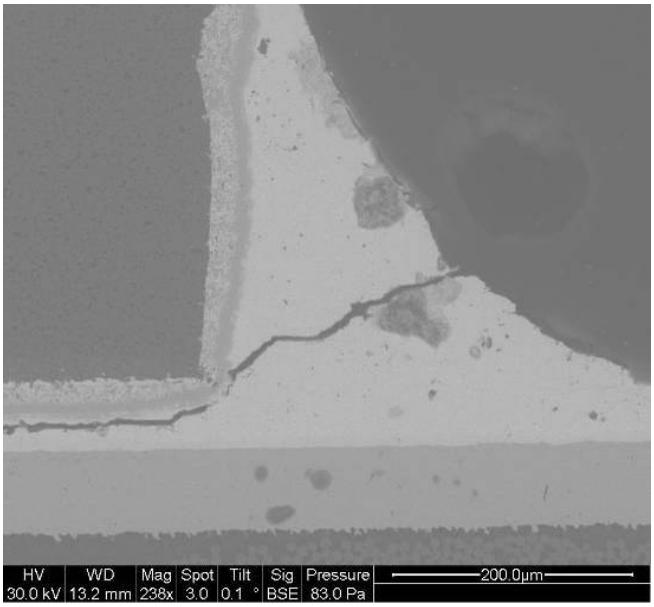

Figure 49. Solder crack of SAC105, resistor 33 (narrow pad), failed at 146,160 cycles

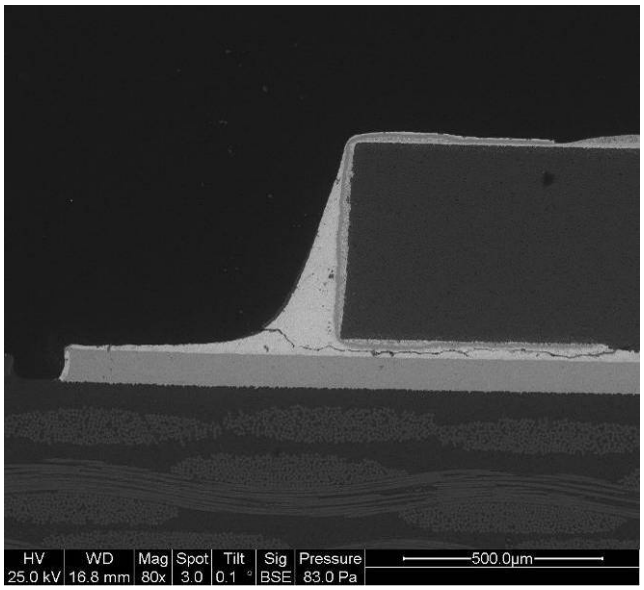

Figure 50. Solder crack of SAC105, resistor 29 (narrow pad), failed at 584,640 cycles

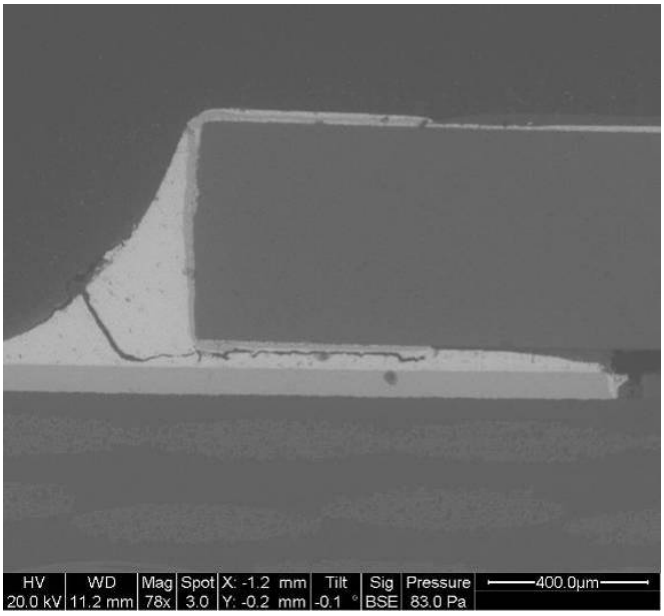

Figure 51. Solder crack of SAC305, resistor 33 (narrow pad), failed at 549,360 cycles

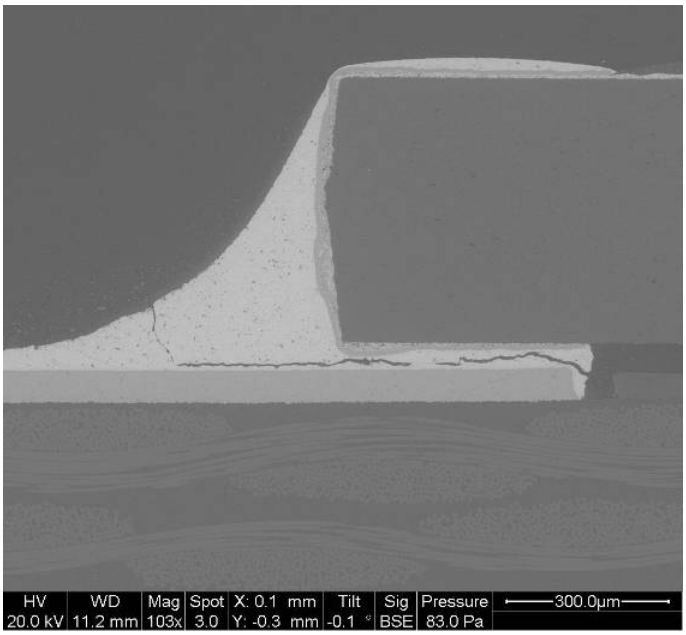

Figure 52. Solder crack of SAC305, resistor 3 (narrow pad), failed at 2,171,280 cycles

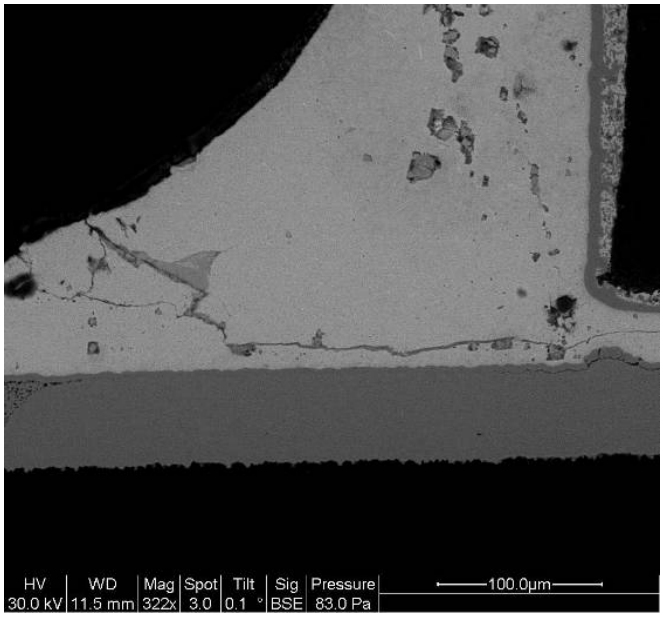

Figure 53. Solder crack of SN100C, resistor 28 (narrow pad), failed at 134,640 cycles

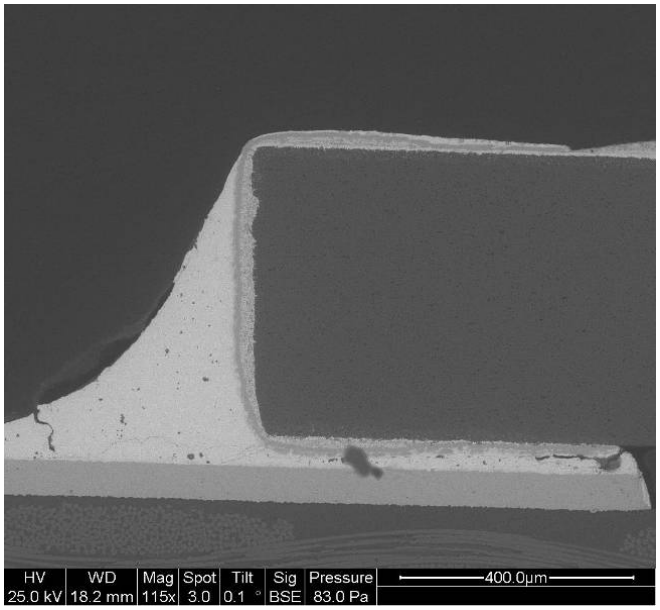

Figure 54. Solder crack of SN100C, resistor 3 (narrow pad), failed at 428,400 cycles

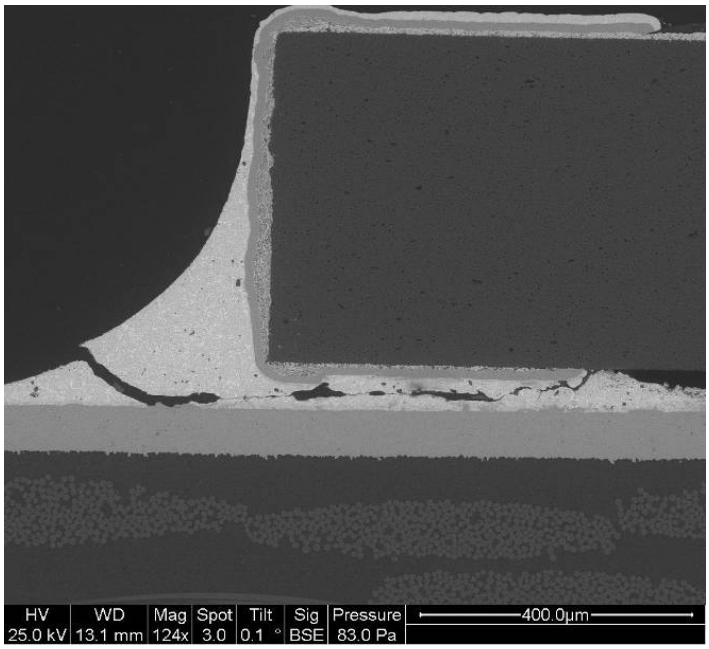

Figure 55. Solder crack of SnPb, resistor 38 (standard pad), failed at 61,266,300 cycles

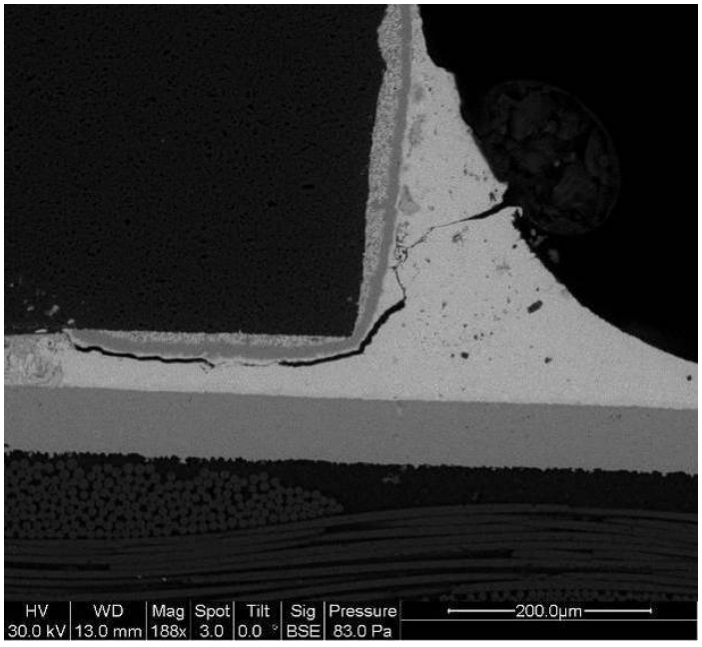

Figure 56. Crack of SAC105, resistor 38 (standard pad), failed at 706,440 cycles

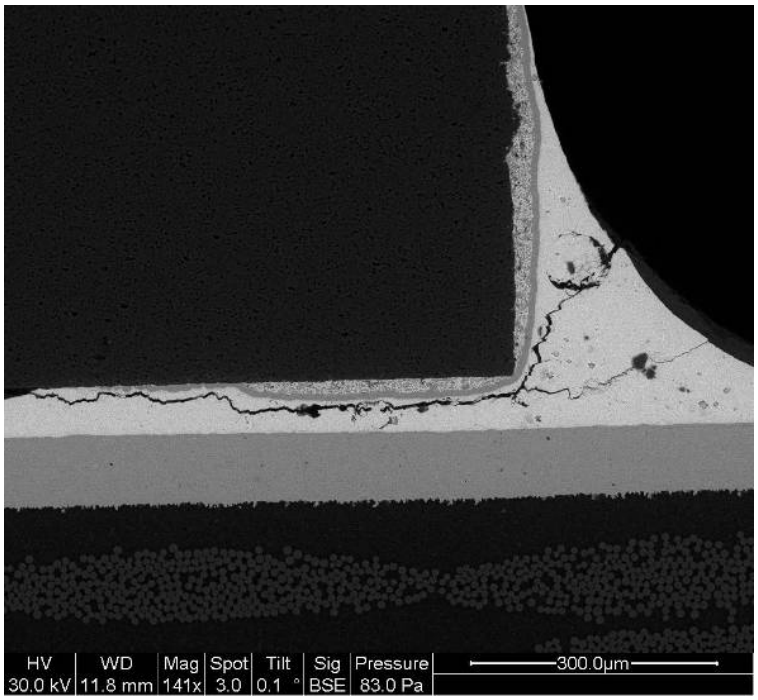

Figure 57. Crack of SAC105, resistor 13 (standard pad), failed at 3,824,520 cycles

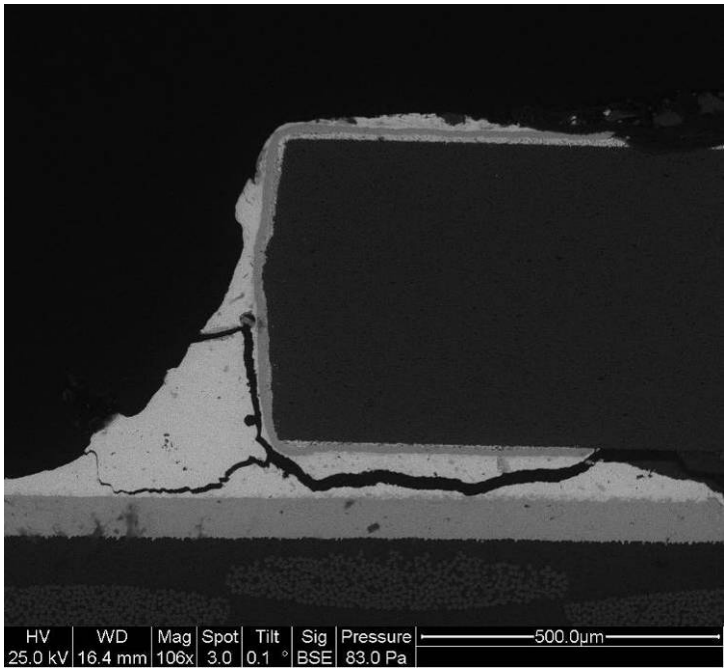

Figure 58. Solder crack of SAC305, resistor 23 (standard pad), failed at 22,440,600 cycles

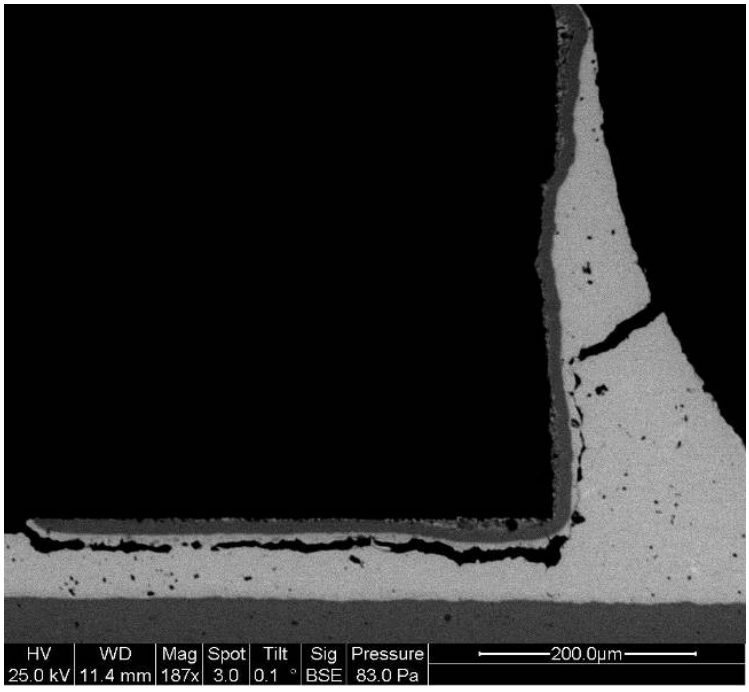

Figure 59. Solder crack of SAC305, resistor 8 (standard pad), failed at 39,551,400 cycles

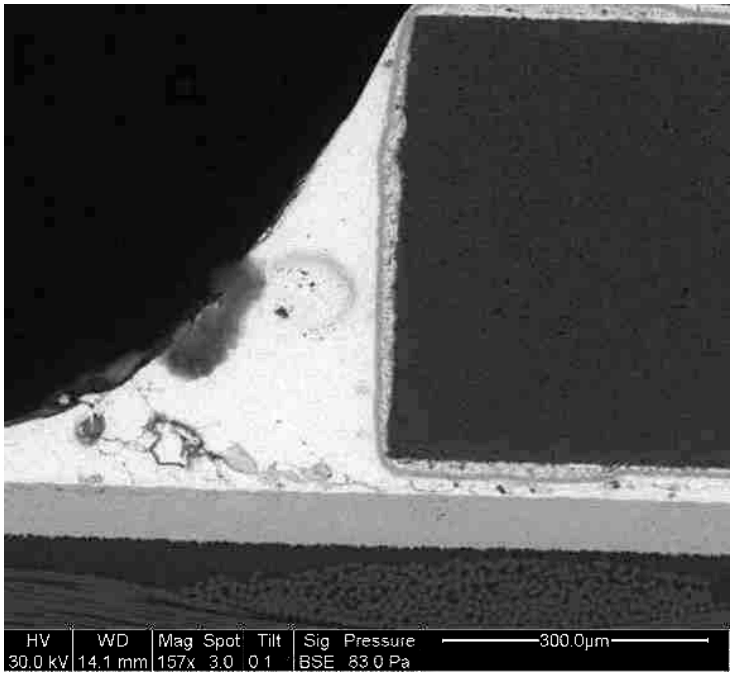

Figure 60. Solder crack of SN100C, resistor 17 (standard pad), failed at 1,321,920 cycles

F. Adjustment for Different Loading Conditions - Goodman Diagram

The following is a description based closel on the calculations from the Goodman Diragram as described in Patrice Gregory's dissertaition [23].

After calculating the interconnect stress range index, the vibration data was still slightly higher than the data from the four point bend tests. This is shown in Figure 61. Durability plot of Gregory's Four point Bend Tests and Vibration BGA tests - Unadjusted. This is expected because the vibration test loading condition was fully-reversed, with a zero-mean stress. The four point bend loading condition was tension-tension with a mean stress that is the stress amplitude. Therefore the data between these two different tests still cannot be compared. In order to compare them, these different loading conditions need to be accounted for. This can be done using a modified Goodman diagram, which is used to find a correlation factor between two different fatigue data sets [24]. This diagram is originally for finding an equivalent endurance limit for a material under conditions of nonzero mean stress, but it can also be used to find the equivalent stress at a specific life under a nonzero mean stress.

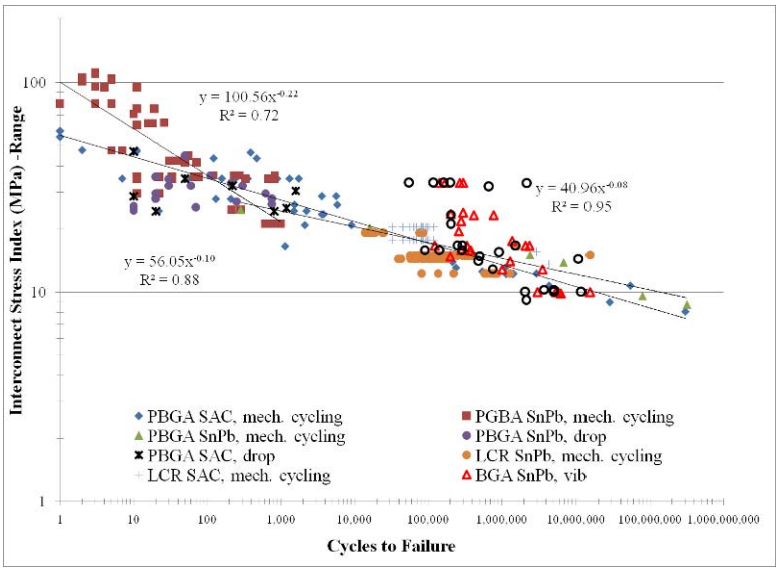

Figure 61. Durability plot of Gregory's Four point Bend Tests and Vibration BGA tests - Unadjusted

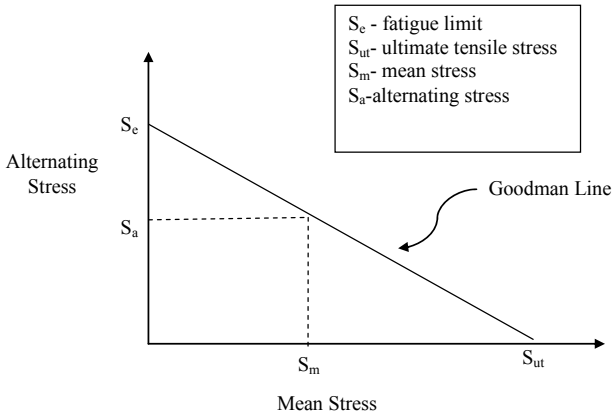

Figure 62. Modified Goodman diagram.

The Goodman diagram, shown in Figure 62, is a plot of the mean stress along the horizontal axis and the alternating stress on the vertical axis. The BGAs discussed in Chapter 3 had a critical stress amplitude for zero mean stress at approximately one million cycles. From the FEA analysis done by Gregory [23], using the measured PWB strain range resulted in a calculated stress index of 11 MPa. The yield strength of the solder is 27.2 MPa, and as stated in Gregory's

dissertation [23], this is the point placed on the horizontal axis of the diagram – since there is no alternating stress amplitude, it is assumed that the solder joint is going to fail when it reaches the critical tensile stress, and in the Goodman diagram, this is deemed the yield strength.

After determining the points on the vertial and horizontal axis, as described above, a line is drawn between the two points. The line represents all the failure states between the zero mean stress and the zero alternating stress amplitude.

In order to determine the ratio of the vibration loading condition to the four point bend loading condition, simple geometry and similar triangles are used. The four point bending loading condition where on the horizontal and verticle axis where the mean stress and alternating stress amplitude are equal to each other are indicated on the diagram. The unknown x is the value of the stress amplitude with an identcal value of mean stress. From similar triangles:

$$\frac{vertical\_length}{horizontal\_length} = \frac{11}{27.2} = \frac{11-x}{x}$$

To adjust the vibration stress index to be an equivalent loading to the 4 point bending stress index, the vibration stress index is reduced by the factor of x/11 which turns out to be about 9/11.

References

[1] Barker, D. and Sidharth. "Vibration-Induced Fatigue Life Estimation of Corner Leads of Peripheral Leaded Components." Transactions of ASME, vol. 118, Dec 1996, pp. 244-249.

[2] Wu, Mei-Ling. "Vibration-Induced Fatigue Life Estimation of Ball Grid Array Packaging." Journal of Micromechanics and Microengineering, vol. 19, no. 065005, 18 May 2009.

[3] Dasgupta, A; Darbha, S; and Ling, S. "Stress Analysis of Surface-Mount Interconnections Due to Vibrational Loading," Journal of Electronics Packaging, vol. 119, Sept 1997, pp. 183-188.

[4] Al-Bassyiouni, M; Dasgupta, A; and Zhou, Y. "Vibration Durability Assessment on Sn3.0Ag0.5Cu and Sn37Pb Solders Under Harmonic Excitation," Journal of Electronics Packaging, vol. 131, no. 011016, March 2009.

[5] Lau, John H. "Solder Joint Reliability of Flip Chip and Plastic Ball Grid Array Assemblies Under Thermal, Mechanical, and Vibrational Conditions." IEEE Transactions on Components, Packaging and Manufacturing Technology - Part B, vol. 19, no. 4, Nov. 1996, pp. 728-735.

[6] Amagai, Masazumi; Kim, YoungBae; and Noguchi, Hiroshi. "Vibration Fatigue Reliability of BGA-IC Package with Pb-free Solder and Pb-Sn Solder." Microelectronics Reliability, vol. 46, 14 April 2005, pp. 459-466.

[7] Chan, Y.C. and Tu, P.L. "Effect of Intermetallic Compounds on Vibration Fatigue of μBGA Solder Joint." IEEE Transactions on Advanced Packaging, vol. 24, no. 2, May 2001, pp. 197-205.

[8] Chen, L.H.; Lan, G.F; Lui, T.S. and Song, J.M. "Resonant Vibration Behavior of Sn–Zn–Ag Solder Alloys." Journal of Alloys and Compounds, vol. 379, 10 Feb 2004, pp. 233-239.

[9] Chua, K.M; Tan, Y.M; and Wang, Z.P. "Board Level Reliability Assessment of Chip Scale Packages." Microelectronics Reliability, vol. 39, 1999, pp. 1351-1356.

[10] Dasgupta, Abhijit and Upadhyayula, Kumar. "Physics-of-Failure Guidelines for Accelerated Qualification of Electronic Systems." Quality and Reliability Engineering International, vol. 14, 1998, pp. 433-447.

[11] Lim, G. H; Lin, R.M; Pang, John H. L; Wang, Z. P; Yang, Q. J; and Yap, F. F. "Reliability of PBGA Assemblies Under Out-of-Plane Vibration Excitations." IEEE Transactions on Components and Packaging Technologies, vol. 25, no. 2, June 2002.

[12] Celik, M and Genc, C. "Mechanical Fatigue or an Electronic Component Under Random Vibration." Fatigue and Fracture of Engineering Materials and Structures, vol. 31, Jan 2008, pp. 505-516.

[13] Harrison, M.R.; Vincent, J.H.; and Steen, H.A.H. “Lead-free Reflow Soldering for Electronics Assembly.” Soldering & Surface Mount Technology, vol. 13, issue 3, Jun 2001, pp. 21-38.

[14] Hung, Fei; Lai, Truan-Sheng; Chen, Li-Hu; and You, Ji-Ge. "Vibration Fatigue Behavior of Sn-9Zn-xCu Lead-Free Solders." Journal of Materials Science, vol. 42, issue 11, Jun 2007, pp. 3865-3873.

[15] Barry, N; Jones, I.P.; Hirst, T; Fox, I; and Robins, J. "High-Cycle Fatigue Testing of Pb-Free Solder Joints." Soldering & Surface Mount Technology, vol. 9, iss. 2, 2007, pp. 29-38.

[16] Lee, Soon-Bok; Kim, Iro; and Park, Tae-Sung. "Fatigue and Fracture Assessment for Reliability in Electronic Packaging." International Journal of Fracture, vol. 150, issue 1-2, Mar 2008, pp. 91-104.

[17] Hung, Fei-Y; Lui, Truan-Sheng; Chen, Li-Hui; and He, Nien-Ting. "Resonant Characteristics of the Microelectronic Sn-Cu Solder." Journal of Alloys and Compounds, vol 457, issue 1-2, Jun 2008, pp. 171-176.

[18] Woodrow, Thomas. "Modeling of the JCAA/JG-PP Lead-Free Solder Project Vibration Test Data." Originally Presented at IPC/JEDEC Global Conference on Lead Free Reliability &Reliability Testing, Boston, MA, April 10-11, 2007.

[19] Tzan, S-R and Chu, S-L. "Characterization of Lead-Free Solder by Reliability Testing." IEEE/CPMT International Manufacturing Technology Symposium, 2000.

[20] Lee, Shi-Wei; Lui, Ben Hoi; Kong, Y.H; Balyon, Bernard; Leung, Timothy; Umali, Pompeo; and Agtarap, Hector. "Assessment of Board-Level Solder Joint Reliability for PBGA Assemblies with Lead-Free Solders." Soldering and Surface Mount Technology, vol 14, issue 3, 2002, pp. 46-50.

[21] Wong, Shaw; Malatkar, Pramod; Rick, Canham; Kulkarni, Vijay; and Chin, Ian. "Vibration Testing and Analysis of Ball Grid Array Package Solder Joints" Electronic Components and Technology Conference, 2007.

[22] CALCE_PWA. Version 4.1. User manual. University of Maryland-College Park.

[23] Gregory, Patrice, Comparison Of Interconnect Failures Of Electronics Components Mounted On FR-4 Boards With Sn37Pb And Sn3.0Ag0.5Cu Solders Under Rapid Loading Conditions, PhD Dissertation, University of Maryland College Park, 2010.

[24] Shigley, Joseph E. and Charles R. Mischke, *Mechanical Engineering Design*, Magraw-Hill, 1989, pp.297-299.

[25] Chauhan, Preeti; Osterman, Michael; Srinivas, Vikram; and Willard, Nicholas. "Board level reliability evaluation of low silver (Ag) content lead-free solder joints at low strain rates." *International Conference on Solder and Reliability*, Toronto, Canada, May 2010.

[26] Osterman, Michael and Abhijit Dasgupta, Life expectancies of Pb-free SAC solder interconnects in electronic hardware, Journal of Materials Science: Materials in Electronics, Volume 18, Numbers 1-3, March, 2007, pp 229-236.

[27] Darveaux, Robert, Coery Reichman, and Nokibul Islam, "Interface Failure in Lead Free Solder Joints," 206 Electronic Components and Technology Conference, pp. 906-917.

[28] Darveaux, R., and K. Banerji, Constitutive relations for tin-based solder joints, IEEE Transactions on Components, Hybrids, and Manufacturing Technology, Vol. 15, Iss, 6, December 1992, pp. 1013-1024.

[29] Qi, Haiyu Qi, Mikyoung Lee, Michael Osterman, Kyujin Lee, Seyong Oh, and Tim Schmidt, Simulation Model Development for Solder Joint Reliability for High Performance FBGA Assemblies, 20th IEEE SEMI-THERM Symposium, 2004

[30] Zhou, Y., and A. Dasgupta, Vibration Durability Assessment of Sn3.0Ag0.5Cu & Sn37Pb Solders under Harmonic Excitation, 2007 ASME International Mechanical Engineering Congress and Exposition, Seattle, Washington, November 11-17, 2007.

[31] Watkins, James, Evaluating the Susceptibility of Electronic Components Assembled with Leaded Solder to Flexural Failures, with High Rate Considerations, PhD Dissertation, University of Maryland College Park, 2008.